

On the Propagation of Ultra-High Energy Cosmic Rays in the local Universe

**(Ausbreitung Ultra-Hochenergetischer kosmischer Strahlung
im lokalen Universum)**

von

Stefan Hackstein

geboren am

12. Februar 1990

Master-Arbeit im Studiengang Physik
Universität Hamburg

2017

- 1. Gutachter: Prof. Dr. Marcus Brüggen**
- 2. Gutachter: Dr. Franco Vazza**

Contents

1. Abstract	3
1.1. Abstract	3
1.2. Zusammenfassung	3
2. Introduction	5
2.1. Sources of CRs	6
2.2. Cosmic Magnetic Fields	7
2.3. Propagation of UHECRs	8
3. Goals	10
4. Framework	11
4.1. Simulation and Datasets	11
4.2. CRPropa	14
4.3. Preliminary Analysis	17
5. Results and Discussion	19
5.1. Energy Spectrum	19
5.2. Composition	22
5.3. Source Contribution	24
5.4. Harmonic Analysis	25
6. Conclusion	28
7. Acknowledgement	31
A. Appendix	40
A.1. Energy Spectrum	40
A.2. Composition	40
A.3. Source Contribution	41
A.4. Angular Power	41

1. Abstract

1.1. Abstract

We use the CRPROPA code to investigate the propagation of ultra high energy cosmic rays in an extended set of magneto-hydrodynamical simulations of cosmic volumes produced with the ENZO code. We explore an unconstrained simulation of the Universe, where we probe the implications of an homogeneous primordial magnetic field with different initial strengths allowed by present observations. We further investigate a constrained simulation that resembles the most prominent local structures, where we test several models for magnetogenesis. We vary a number of input parameters to find their influence on the observables of ultra high energy cosmic ray measurement, namely the energy spectrum, the composition and the distribution of arrival directions. The varied parameters are the position of the observer in the unconstrained simulation, the set of sources of cosmic rays, the strength and genesis of extragalactic magnetic fields as well as the composition of cosmic rays injected by their sources. We argue that given the latest observational constraints on extragalactic magnetic fields, ultra high energy cosmic ray astronomy will be possible with a full-sky coverage and sufficient number of particles observed at energies above 10^{20} eV, even if dominated by heavy nuclei. We further find that strong magnetic fields around the observer can result in an anisotropic signal at a few EeV which is in conflict with observations. This feature can be used to discard models of magnetic field seeding processes.

1.2. Zusammenfassung

Wir nutzen den CRPROPA-code zur Erforschung der Ausbreitung ultra-hochenergetischer kosmischer Strahlung in mehreren magneto-hydrodynamischen Simulationen kosmischer Volumina, welche mithilfe des ENZO-codes erstellt wurden. Wir erforschen in einer mit unserem Universum vergleichbaren Simulation die Auswirkungen eines homogenen primordialen magnetischen Feldes mit unterschiedlicher Feldstärke innerhalb der durch derzeitige Beobachtung erlaubten Grenzen. Weiter untersuchen wir verschiedene Modelle der Magnetogenesis in einer Simulation in der wir die bedeutendsten Strukturen unseres Universums wiederfinden. Wir verändern mehrere Anfangsparameter um deren Einfluß auf die Observablen der Messung ultra-hochenergetischer kosmischer Strahlung zu erkennen. Diese Observablen sind das Energiespektrum, die Zusammensetzung der kosmischen Strahlen sowie die Verteilung derer Ankunftsrichtungen. Die veränderten Parameter sind die Position des Beobachters, die Wahl der Quellen kosmischer Strahlung, Stärke und Ursprung extragalaktischer Magnetfelder sowie die von den Quellen emittierte Zusammensetzung kosmischer Strahlung. Wie zeigen auf, dass mit extragalaktischen Magnetfeldern in Übereinstimmung mit aktuellen Beobachtungen die Astronomie mit ultra-hochenergetischer kosmischer Strahlung möglich wird durch die Messung genügend vieler Teilchen über den gesamten Himmel mit Energie $> 10^{20}$ eV, auch wenn schwere Atomkerne diesen Energiebereich dominieren. Weiter finden wir, dass starke Magnetfelder in der nahen

1. Abstract

Umgebung des Beobachters ein anisotropes Signal bei einer Energie von einigen EeV erzeugen können, welches nicht mit Beobachtungen vereinbar ist. Dieses kann genutzt werden um Modelle von Prozessen der Erzeugung magnetischer Felder auszuschließen.

2. Introduction

The study of cosmic rays (CRs), since their discovery by Viktor Hess in the 1910s (F. Hess 1912), has led to a great number of developments in modern physics. Measurements of the “Höhenstrahlung”, as it was called back then, led to the discovery of antimatter (Anderson 1932), boosting the development of the standard model of particle physics. CRs are a direct probe of the most powerful particle accelerators in the Universe that surpass the energies produced at the Large Hadron Collider or other man-made accelerators by several orders of magnitude.

At low energies ($\lesssim 10^{17}$ eV), the detection of CRs is rather simple as they can be measured directly using particle detectors like e. g. cloud chambers as has been done by Hess and many others since the beginning of the last century (e. g. Hörandel 2013). At higher energies, CRs can interact with our atmosphere and induce extensive air showers of particles and electromagnetic radiation. The detection of these air showers is more difficult and demands combined arrays of particle and radiation detectors. Only few of such showers occur per square kilometre per year; huge detector arrays are required to measure enough high energy CR events to overcome statistical uncertainties. Some of the biggest and most sophisticated detector arrays that have been build so far are the Pierre Auger Observatory¹ (PAO) in Argentina and the Telescope Array² (TA) in the U. S. A..

In the coming decade the PAO will expand to the northern hemisphere with another huge array of detectors in Colorado, U. S. A., which is more than 3 times larger than the southern site (e. g. Nitz 2008). Not only will this additional huge observatory allow for a more frequent observation of CRs at the highest energies, the completion of the northern site will mark the transition to an era of full-sky coverage of UHECR observation, mandatory for certain measurements of anisotropies in the arrival directions.

The CRs are predominantly charged nuclei that arrive at Earth with energies from 10^8 eV up to a few 10^{20} eV. The energy spectrum can be well described by a power law of index $\alpha \simeq -2$ over 11 magnitudes. At about 10^{15} eV the spectrum slightly steepens and forms the so called “knee”, which is likely to indicate the maximum acceleration energy for light nuclei in galactic sources. At about 10^{18} eV the energy spectrum flattens which is believed to mark the transition from galactic to extragalactic sources. This feature is generally referred to as the “ankle”.

All types of nuclei are measured over the whole energy spectrum of CRs, but the overall composition changes with energy. At low energies ($\lesssim 10^{15}$ eV), most of the CRs are Hydrogen nuclei. Above 10^{15} eV the composition becomes heavier and around 10^{17} eV it is dominated by iron. At a few 10^{18} eV the composition is again dominated by protons (Dova 2016). For even higher energies several observatories show conflicting results: while TA measurements

¹www.auger.org

²www.telescopearray.org/

2. Introduction

from the northern hemisphere suggest a proton dominated composition, PAO on the southern hemisphere reports a transition to heavier nuclei at the highest energies (Abbasi et al. 2016.) (for more extensive reviews see e. g. Bhattacharjee 2000; Blasi 2013; Kotera and Olinto 2011; Letessier-Selvon and Stanev 2011; Nagano and Watson 2000).

The high isotropy of the CR signal at high energies allows to estimate the strength of the galactic magnetic field (GMF) of the Milky Way (MW) to be a few μG , which has been confirmed by more direct ways of measuring (e. g. Haverkorn 2015). The gyro-radius of a charged particle in a homogeneous field is

$$r_g = \frac{E}{eZB} \approx \frac{110 \text{ kpc}}{Z} \left(\frac{E}{100 \text{ EeV}} \right) \left(\frac{B}{\mu\text{G}} \right)^{-1},$$

where E is the energy of the particle, Z its charge number and B the magnetic field. At energies below 10^{17} eV, the gyro-radius of CRs in an homogeneous magnetic field with strength B of the order of a few μG is less than the height of the MW of a few kpc. CRs below this energy are confined within their host galaxy and have to originate inside the MW. On the other hand, at energies above 10^{19} eV ultra high energy cosmic rays (UHECRs) are rigid enough to escape the GMF of the host galaxy. If those UHECRs originated within the MW, a strong correlation between their arrival directions and the galactic plane is expected; no such correlation has been found. This indicates the transition from galactic to extragalactic sources somewhere between $10^{17} - 10^{19}$ eV.

2.1. Sources of CRs

The most plausible galactic sources of CRs at energies $\lesssim 10^{17}$ eV are shocks in the remnants of super novae, where charged particles diffusively accelerate in variable magnetic fields, a process called Fermi acceleration (e. g. Blasi 2013). A particle can only accelerate as long as it is confined within the source. This limits the energy of particles a source can emit. The energy limit is obtained by equating the gyro-radius with the size of the source

$$E_{\text{max}} < ZeBr_{\text{source}},$$

as proposed by Hillas (1984). He produced a famous plot that distinguishes the only known objects that possibly are the sources of UHECR protons at the highest energies, i. e. AGN (esp. radio galaxies, quasars and BL Lacs), Gamma Ray Bursts (GRBs) and shocks in galaxy clusters (Hillas 1984; Ptitsyna and Troitsky 2010).

The possible extragalactic sources of UHECRs can be grouped in two categories. For the *transient* sources the emission lifetime is shorter than the spread in arrival time due to magnetic deflection, the UHECRs arrive at the Earth long time after we could observe the expiration of the source in the electromagnetic radiation. The *steady* sources last much longer and are still

2. Introduction

visible when the emitted particles arrive at Earth. The latter happen to be relatively common and can be found in virtually any galaxy, e. g. GRBs and fast-rotating neutron stars. Steady sources are objects that are rarely found throughout the universe, e. g. radio galaxies and quasar remnants (Fang and Kotera 2016; Kotera and Olinto 2011). The PAO has reported lower bounds on the density of steady sources of $\gtrsim 10^{-4} \text{ Mpc}^{-3}$ due to the absence of anisotropy in the arrival directions of UHECRs (Abreu et al. 2013).

2.2. Cosmic Magnetic Fields

Cosmic magnetic fields (CMFs) are believed to reside in all structures found throughout the Universe. Since CMFs cannot be observed directly, accurate measurements of these fields are rather difficult and demands sophisticated techniques and advantageous conditions (e. g. Kronberg 1994). To this day CMFs are measured only in a very restricted portion of cosmic structures, i. e. galaxies and a few clusters.

The major part of the Universe ($\sim 80\%$ of volume) is taken by voids, which are sparsely inhabited by galaxies. Recent observation of the cosmic microwave background (CMB) by the PLANCK-mission put an upper limit on the strength of a primordial magnetic field by analyzing the angular power spectra of the CMB (Ade et al. 2015). This translates to an upper limit on the strength of magnetic fields in voids of $\sim 1 \text{ nG}$, since additional magnetic field seeding processes scale with the mass density. It has been argued that the non-gaussianity of the CMB signal could further decrease this limit (Trivedi, Subramanian, and Seshadri 2014). A lower limit on the magnetic field strength in voids of $\sim 10^{-7} \text{ nG}$ has been proposed due to the lack of secondary emission around blazar sources (Neronov and Vovk 2010).

The large scale structure (LSS) is build by clusters of galaxies that are connected by filaments and form a honey-comb-like structure around the voids. Virtually all galaxies host GMFs with typical strength of $\sim 5 - 15 \mu\text{G}$, which were measured using Faraday rotation and synchrotron emission (e. g. Vallée 2004). While future radio observations will offer the chance to measure the magnetization of filaments and the outskirts of clusters (Vazza et al. 2015), not much is known about it today. UHECRs are sensitive to those extragalactic magnetic fields (EGMFs) and therefore offer a chance to measure their characteristics. In this thesis we investigate the possibility to use UHECRs to measure magnetic fields that reside outside the MW.

The origin of CMFs is yet unclear. Several scenarios have been proposed, but we lack evidence to decide which of these took place in our Universe. The generation of primordial magnetic fields has been proposed e. g. during cosmic inflation, phase transitions or baryogenesis or by Biermann batteries during reionization (e. g. Gnedin, Ferrara, and Zweibel 2000; Subramanian 2015; Widrow et al. 2012). These fields evolve over time, they are influenced by the formation of structure, they are damped by cosmic expansion and finally they should be amplified by dynamo processes in dense structures. Other models propose the generation of CMFs from astrophysical processes like magnetized galactic winds (e. g. Bertone, Vogt, and Ensslin 2006; Donnert et al. 2009) and active galactic nuclei (AGN, e. g. Xu et al. 2009). In

this thesis we simulate idealised versions of the above competing scenarios for the origin of CMFs and assess their impact on the propagation of UHECRs.

2.3. Propagation of UHECRs

Fully ionized UHECR nuclei that travel across the cosmic volume undergo a number of interactions that can be grouped by the effect they have on the nucleus. CMFs act on UHECRs via the Lorentz Force, altering the direction of movement of the nuclei. This deflection forces the nuclei to travel longer before they reach the observer

$$\Delta t \approx 10^5 \text{ yr} \left(\frac{d}{100 \text{ Mpc}} \right) \left(\frac{\theta}{2^\circ} \right), \quad (2.1)$$

where d is the distance to the source and θ the total deflection angle (Kotera and Lemoine 2008).

Energies $> 10^{18}$ eV are sufficient to allow for production of pairs of particles in interaction with ambient photon fields³ on a rather short time scale causing a slow energy loss of the nucleus (e. g. Kotera and Olinto 2011). Above $5 \cdot 10^{19}$ eV, called the GZK-limit, protons might interact with CMB photons and produce pions via Δ -resonance as proposed independently in Greisen (1966) and Zatsepin and Kuz'min (1966). This interaction has a much longer mean free path than pair production but causes a much stronger loss of energy, which led to the prediction of the so called GZK-cut-off expected at energies of about 10^{20} eV. No UHECR nucleus could reach the Earth with energies exceeding that limit, since it would lose its energy on the way. Confirmation of the GZK-cut-off has been reported by the High Resolution Fly's Eye experiment (Abbasi et al. 2008) and the PAO (Abraham et al. 2008); it remains unclear whether this cut-off coincides with the maximum injection energy of UHECR sources. Furthermore, the GZK-effect limits the maximum travelled distance of UHECRs above the GZK-limit to ~ 100 Mpc. This constrains their sources to the local Universe and may allow for UHECR astronomy at the highest energies with a possibly anisotropic signal.

For heavy UHECR nuclei, energy losses are more severe and the energy loss length increases with the mass of the nucleus (e. g. Bertone et al. 2002). Heavy nuclei can further “lose” their nucleons, not only by regular α - and β -decay. When hit by a photon of the ambient background radiation they can also photo-disintegrate

$$A + \gamma \rightarrow (A - 1) + n,$$

where A is a nucleus compiled of A nuclei and n is a nucleon. In such processes the initial energy is on average distributed evenly among the nucleons, which causes an energy loss more dominant than the processes in the previous paragraph. In fact, iron nuclei above $2 \cdot 10^{20}$ eV are likely to lose their energy together with most of their nucleons within less than 10 Mpc, as was

³the CMB, the infra-red background and to a small extend visible light.

2. Introduction

shown in Epele and Roulet (1998) and Khan et al. (2005). A stronger magnetic field increases the effectively travelled distance raises the probability for photo-disintegration, a lighter composition is expected (e. g. Bertone et al. 2002). For a very detailed review on the propagation processes of heavy nuclei see e. g. Allard (2012).

3. Goals

This thesis will investigate

- the propagation of UHECRs in unconstrained as well as constrained MHD models with structured CMFs;
- the possibility to constrain CMFs using full sky observation of UHECRs;
- the influence of different source distributions on UHECR measurements.
- implications of an injected CR composition on UHECR measurements;

4. Framework

mnemonic	generation of magnetic field	L_{box} [Mpc]	N_{grid}	Δx [kpc]
<i>UCS(+1...+6)</i>	$B_0 = 10^{-(14...8)}\text{G} + \text{AGN}(10^{57}\text{erg}), e_B = 10\%$ cooling, star formation	100	512^3	195
$B=0$	non-radiative, no magnetic field	250	1024^3	(44) 244
<i>astrophysical</i>	$\text{AGN}(10^{59}\text{erg}), e_B = 50\%$, cooling	250	1024^3	(44) 244
<i>primordial</i>	non-radiative, $B_0 = 10^{-9}\text{G}$	250	1024^3	(44) 244

Table 1: List of magnetic field models investigated in this thesis, the line separates the realizations in the UCS (top) and the CS (bottom). First column: name of the model, volume; second column: physical module; third column: box length of the simulated ; fourth column: number of grid cells in the initial conditions; fifth column: spatial resolution, the values in brackets show the maximum resolution achieved at run time.

4. Framework

4.1. Simulation and Datasets

The simulations analyzed in this work have been produced with the grid code ENZO (The Enzo collaboration 2013), which is a highly parallel code for cosmological magneto-hydrodynamics (MHD), which uses a particle-mesh N-body method to follow the dynamics of the Dark Matter and a variety of shock-capturing Riemann solver to evolve the gas component (Bryan et al. 2014). The MHD simulations we present here employed the Dedner formulation of MHD equations (Dedner et al. 2002) which uses hyperbolic divergence cleaning to preserve $\nabla \cdot B = 0$. The MHD solver uses the Piecewise Linear Method reconstruction, where fluxes at cell interfaces are calculated using the local Lax-Friedrichs Riemann solver (Kurganov and Tadmor 2000) and time integration is performed using the total variation diminishing second order Runge-Kutta scheme (Shu and Osher 1988). In addition to gravity and MHD, our runs included metallicity-dependent equilibrium gas cooling, star formation and feedback (Cen and Ostriker 1992). These simulations also made use of the recent porting on CUDA into the Dedner algorithm, in order to efficiently run on the GPU (Li et al. 2010), which runs ~ 4 times faster on GPU, compared to the performance on CPUs. This suite of runs belongs to a larger suite of MHD cosmological simulations (‘CHRONOS++’), designed to investigate the origin of EGMFs (Vazza et al. 2014, 2015).

This thesis combines the results of two slightly different campaigns of simulations, meant to focus on different aspects of UHECR propagation and cosmic magnetism. The first is a set of Unconstrained Simulations (UCS) where we simulated the evolution of a $(100 \text{ Mpc})^3$ comoving volume, which has been simulated from $z = 30$ to 0 on a fixed grid of 512^3 cells and using 512^3 dark matter particles with homogeneous distribution in the initial state. In order to investigate the whole range of allowed magnetic field strengths in voids, we renormalized the uniform initial value along each axis from $B_0 = 10^{-14}\text{G}$ to 10^{-8}G in logarithmic steps to base 10. Our main goal in using this set of simulations is to test trends of UHECRs propagation with magnetic fields of increasing strength, as well as to closely connect to our previous results in

4. Framework

Hackstein et al. (2016), which were presented for a pure proton composition only. There we concluded that due to strong cosmic variance the use of constrained simulations is mandatory to form firm conclusions on the measure of magnetic fields with the use of UHECRs. We therefore investigate a second set of newer Costrained Simulations (CS) of the local Universe, obtained from the initial conditions produced by J. Sorce and collaborators (CLUES collaboration⁴, Sorce et al. 2016). In this second set of simulations we sampled a larger volume of $(500 \text{ Mpc})^3$ with 512^3 cells and dark matter particles, and applied adaptive mesh refinement to further refine by a factor 32 the innermost $(200 \text{ Mpc})^3$ volume in order to form clusters that closely resemble real local structures (e.g. the Centaurus, Virgo, Coma and Perseus clusters). For further details on how these initial conditions were produced we refer the reader to Sorce et al. (2016). In this work, we explored for the first time the simulation of these initial conditions with ENZO and using MHD. In order to obtain a more realistic magnetic field in the nearby clusters we increased the efficiency of the magnetic energy feedback e_B from $e_B = 1\%$ in the UCS to $e_B = 50\%$ in the CS. This choice is the result of further investigation in the years between the production of the two sets of simulations. Due to the limited size of computer memory we restricted the simulations in CRPROPA to the innermost $(250 \text{ Mpc})^3$ volume of the CS.

In the CS we realized several different models for the origin of CMFs. To obtain the *primordial* model we set a uniform field of $B_0 = 10^{-9} \text{ G}$ along each coordinate axis at $z = 30$, like in the UCS. To realize the generation of CMFs by *astrophysical* processes, at $z = 1$ we allowed for the impulsive thermal and magnetic feedback in haloes, where the physical gas density exceeded the critical value of $(10 \text{ cm})^{-3}$, which marks the onset of catastrophic gas cooling. The magnetic energy is always assumed to be 50% of the injected thermal energy. While the thermal energy is released as a couple of over-pressurized outflows at random opposite directions from the halo centre, the feedback magnetic energy is released as dipoles around the centre. Finally, we used the same simulation without magnetic fields, $B=0$, as a control run. An overview on all magnetic field models investigated in this thesis can be found in Tab. 1. All these models do only contain the regular component of the CMFs, since their resolution is too sparse to reproduce the turbulent component in detail.

In the simulations explained above we realized different sets of sources of UHECRs. To realize the most isotropic injection case we chose random positions with an *homogeneous* distribution in the simulated volume. We further identified the centres of *mass halos* where the gas density exceeds the average density by a factor of 20, which marks the usual viral density of halos in the universe. These give the positions where we are most likely to find high energetic, long-living objects and are therefore a realization of steady sources. These two injection scenarios are realized in both, the UCS and the CS. The mass resolution of dark matter particles in the CS is about 125 times worse than in the UCS. This means that only halos of larger mass can be properly resolved in the CS.

⁴<https://www.clues-project.org/cms/>

4. Framework

mnemonic	injection scenario	L_{box} [Mpc]	N_{sources}	n_{sources} [Mpc $^{-3}$]
<i>homogeneous</i>	random positions, homogeneous distribution	100	10^7	10
<i>mass halo</i>	viral halos	100	329	$3.29 \cdot 10^{-4}$
<i>homogeneous</i>	random positions, homogeneous distribution	250	10^7 (10^8)	0.64 (6.4)
<i>density</i>	random positions, follow gas density	250	10^7 (10^8)	0.64 (6.4)
<i>mass halo</i>	viral halos	250	2672	$1.71 \cdot 10^{-4}$
<i>vcv_velzen</i>	positions of RG & AGN in VCV and Velzen	250	1702	$1.09 \cdot 10^{-4}$

Table 2: List of injection scenarios realized in this thesis, the line separates the realizations in the UCS (top) and the CS (bottom). First column: name of the scenarios; second column: set of sources; third column: box length of the simulated; fourth column: number of sources in the simulated volume; fifth column: number density of sources. The numbers in brackets show the case of pure proton injection.

A more realistic set of steady sources in the UCS was compiled with the coordinates of objects in the Véron–Cetty & Véron catalogue of AGN (Véron-Cetty and Véron 2010) as well as in the van Velzen catalogue of radio galaxies (van Velzen et al. 2012) in the real Universe; objects that appear in both catalogues have been considered only once. The number density of sources in the merged *vcv_velzen* set is slightly below the *mass halo* case, right at the border of what is allowed by the constraints of $\sim 10^{-4} \text{Mpc}^{-3}$ given by the PAO (Abreu et al. 2013). This reflects the incompleteness of the catalogues, especially where the view is blocked, e. g. by the centre of our galaxy.

In order to have a maximum possible source density that follows the large scale structure, we further injected at random positions with a probability distribution function that is identical to the gas *density*. The probability distribution function is renormalized, such that the integral over the whole volume is identity, the maximum injection probability is at high density peaks and ten times lower density means ten times fewer injections. This reflects the case of transient sources that may happen in any galaxy. An overview on all injection scenarios is given in Tab. 2.

The injection of protons with energies in the range of 10^{18} eV to 10^{21} eV from viral haloes in the UCS has been analyzed in Hackstein et al. (2016); in this thesis we extend this analysis by injection of a pure iron composition from the same set of *mass halo* sources. To investigate the influence of the distribution of sources in the UCS, we further used *homogeneous* sources in the two strongest models, UCS+5 and UCS+6.

In the CS we injected a pure proton as well as a pure iron composition from 10^{18} eV to 10^{21} eV in all 12 combinations of magnetic field models and injection scenarios. Due to the increased size of the simulated volume, the effective number of observed particles is reduced strongly in the CS; The pure iron injection scenarios result in very low number statistics (< 50 particles) for energies above the GZK-limit. In order to investigate the high energy regime, we produced another set of simulations where we injected in the $B=0$ and *primordial* models a pure iron composition and only considered particles above $2 \cdot 10^{19}$ eV.

4.2. CRPropa

In this thesis we made use of CRPROPA 3.0⁵ (Armengaud et al. 2007; Batista et al. 2016; Kampert et al. 2013), which is a publicly available code to simulate the propagation of UHE-CRs. CRPROPA works by injecting nuclei with random initial momentum into a given 3D CMF model, compute their propagation, decay and energy losses. The path of propagation of CRs is then calculated stepwise by integrating the Lorentz equations and computing interactions as well as decay. Pair production is realized as a continuous energy loss $\frac{dE}{dt} = \alpha$, where α is a complex function that entails e. g. the Thomson cross section, particle masses and the temperature of the ambient photon fields; further details can be found in Puget, Stecker, and Bredekamp (1976). Pion production is computed with the use of the cross sections for photo-pion production for free nucleons obtained in experiments, the cross sections of nuclei are then calculated as a superposition of their nucleons. The detailed outcome of pion production processes is calculated with SOPHIA⁶, a Monte Carlo event generator designed to study this phenomenon that first determines the cross sections for all production channels and subsequently subtracts the energy of produced particles (Mucke et al. 2000). Energy loss due to adiabatic expansion can be described as $-\frac{1}{E} \left(\frac{dE}{dt} \right)_{\text{adiabatic}} = H_0$, where H_0 is the Hubble-constant (e. g. Kuempel 2014); it is calculated post-processing by reducing the momentum by factor $(1+z)^{-1}$, where z is the cosmic redshift obtained for every particle by integrating the time evolution

$$\left| \frac{dt}{dz} \right| = \frac{1}{H_0(1+z)\sqrt{\Omega_m(1+z)^3 + \Omega_\Lambda}}$$

To simulate photo-disintegration of heavy nuclei, the mean free path is calculated with the use of the cross section of this process; the loss of energy of the primary nucleus is related to the loss of nucleons by $\frac{1}{E} \frac{dE}{dt} \Big|_{\text{eff}} = \frac{1}{A} \frac{dA}{dt}$ (Kuempel 2014). The decay rate of unstable nuclei is obtained by transforming the half-life times from the rest-frame into laboratory-frame.

When a particle enters a sphere around the observer it is recorded by CRPROPA, the energy, momentum, position and composition of that particle at observation and at injection as well as the travelled distance are written in the output file. CRPROPA also allows to track the path of propagation of particles. In this case, the observables are recorded at every step of calculation.

CRPROPA allows for very detailed and extensive simulations (Alves Batista et al. 2015), though it comes on the cost of high computation times, especially in areas of strong magnetic field, where calculations are performed with higher precision. In this thesis we analyzed 40 CRPROPA runs which took a total of $\sim 2.7 \cdot 10^3$ computation hours on a hexa-core processor at 3.50 GHz with 32 GB memory.

⁵<https://crpropa.desy.de>

⁶Simulations Of Photo Hadronic Interactions in Astrophysics

4. Framework

To cope with the limited size of the 3D models of CMFs, CRPROPA can assume periodicity so if a particle exits the volume it continues on the opposite side; this can result in artificial anisotropies. Since particles from distant sources encounter significant deflections, this effect is removed almost completely by CMFs (Armengaud, Sigl, and Miniati 2005).

Compared to typical length scales for propagation of UHECRs the size of the Earth vanishes; an ideal observer should be point-like. In a simulation such an ideal observer is impossible to realize, since it is incapable to receive particles. On the other hand, an observer sphere with finite size can produce artificial deflections for particles from nearby sources, as pointed out in Hackstein et al. (2016) and Armengaud, Sigl, and Miniati (2005). An additional effect of the finite observer arises with the use of a heavy injection component.

Heavy nuclei at high energies disintegrate as they travel through the ambient photon fields. In absence of magnetic fields, the resulting shower of remnant particles would not spread very much due to the extremely high Lorentz factor of the initial particle. An ideal observer can measure only a single one of those particles, while a finite observer is able to observe several of the remnants. This causes a strong excess of particles in direction of the most nearby sources (cf. Fig. 4.1). In sufficiently strong magnetic fields, several of the remnant particles are allowed to reach even the ideal observer, since they are deflected and thus the shower can be focused on the observer; The finite observer still measures an excess of particles from nearby sources with reduced alignment of their arrival directions. The implications on the observables of UHECRs are discussed in further detail in Secs. 5.1, 5.2, 5.3 and 5.4.

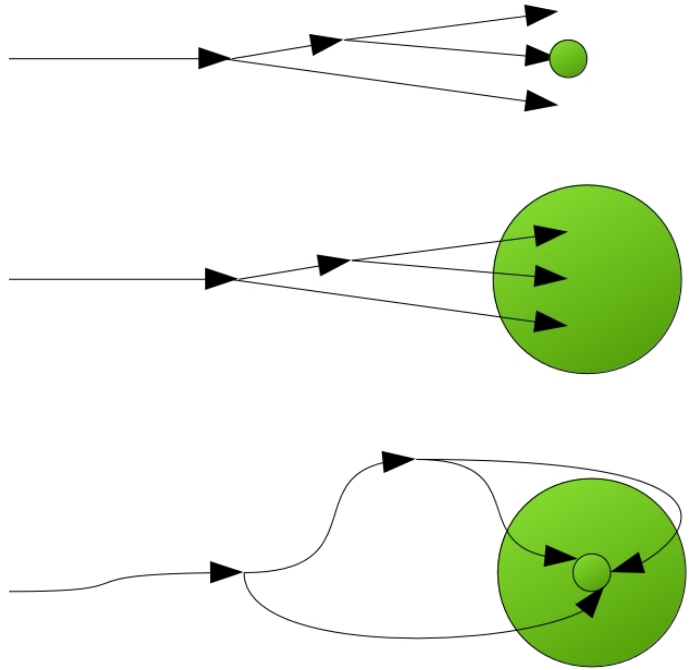


Figure 4.1: Schematic view on the observation of remnant showers of heavy UHECR nuclei in case of the ideal observer (top), a finite observer (center) and a magnetized observer (bottom).

4. Framework

The following is the list of settings used in CRPROPA for the simulations presented in this thesis. We chose these settings in order to get a meaningful set of simulations in feasible computation time and to best cope with the drawbacks of the simulation mentioned above:

```
minStep = 10. kpc
maxStep = 4. Mpc
MaximumTrajectoryLength = 4000. Mpc
observerSize = 0.8 Mpc
Emin = 1 EeV and 20 EeV, respectively
Emax = 1000 EeV
SpectralIndex = -1
Z = 1 and 26, respectively
A = 1 and 56, respectively
Boxsize = 100 Mpc and 250 Mpc, respectively
```

The spectral index α of the injected spectrum $\propto E^\alpha$ was set to $\alpha = -1$. This choice is not expected to reproduce the observed spectrum, which would demand a softer injection spectrum, but results in a bigger number of events at the highest energies, where increased number statistics are needed.

The maximum length for a particle trajectory has been restricted to 4 Gpc in order to reduce computation time. Particles from farer distances have lost most of their initial energy and contribute only to the lower energies. The distribution of sources at such length scales is homogeneous so an observer receives an isotropic signal at those energies even for the chosen maximum length of trajectories.

All runs with CRPROPA were produced on Golem⁷ and the LOFAR GPU cluster⁸, both computing clusters owned by the University of Hamburg. These simulations result in extended lists of information on the arrival direction, energy and composition of UHECR events. Combined, these information form observables that can be analyzed and compared to real data, namely the energy spectrum (Sec. 5.1), the composition of arriving particles (Sec. 5.2) and anisotropy in the arrival directions (Sec. 5.4). We further present the contribution of sources to the observed events (Sec. 5.3), which is not directly measurable but is important in the interpretation of observables and highlights the physical processes in action. All the graphs and figures have been produced from the raw output of ENZO and CRPROPA with use of original algorithms written in IDL⁹ (e. g. Bowman 2005). A representative sample of these routines is given in the Appendix.

4. Framework

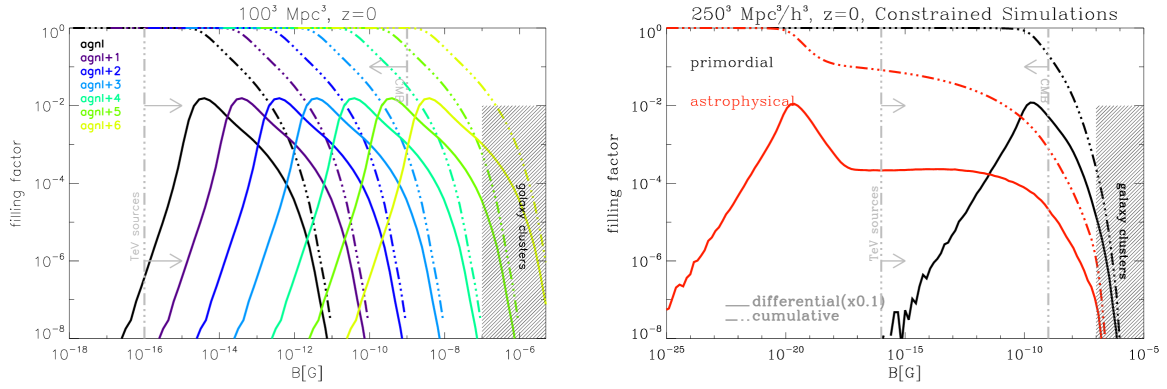


Figure 4.2: Volume filling factor of CMFs in the UCS (left) and CS (right). Shown are the differential (solid) and the cumulative filling factor (dash-dotted). The solid line is multiplied with $\times 0.1$ for more clarity. We also show the constraints given from observations, see Sec. 2.2. The left plot is taken from Hackstein et al. (2016).

4.3. Preliminary Analysis

In Fig. 4.2 we show the volume filling factor of the magnetic field models investigated in this thesis. We present the differential filling factor, i. e. the amount of the volume that contains fields of the give strength, as well as the cumulative one, which sums up the differential factor for fields above the given strength.

The filling factors in the UCS (left panel) are all in well agreement with constraints on magnetic field strengths in voids, except for the strongest model UCS+6. Since additional seeding by astrophysical processes is assumed to be very weak in these simulations, only the two strongest models, UCS+5 and UCS+6, show field strengths in the most strongly magnetized regimes that fit with observations of magnetic fields in galaxy clusters. Together, the models in UCS span over all the field strengths allowed in voids by observational constraints (cf. Sec. 2.2) and are therefore well suited to test the influence of different field strengths and possibly measure magnetic fields in voids. We remark that the application of these models is strictly restricted to the deflection of UHECRs in voids and filaments - due to colometric reasons these are expected to contribute to most of the deflection - while in most cases the fields are inconsistent with observations in galaxy clusters.

In the CS (right panel) we see a clear difference between the *primordial* and the *astrophysical* model. The former is qualitatively similar to the strongest UCS, it agrees with constraints on void fields and with observations in galaxy clusters. The latter consists mainly of the strong fields found in clusters while most of the void volume is essentially free of magnetic fields. With the *primordial* model we investigate the influence of ubiquitous magnetic fields in voids that originate in the early Universe; the *astrophysical* model shows the contribution of magnetic fields from other seeding scenarios in the dense structured parts of the Universe. They are well

⁷<http://www.hs.uni-hamburg.de/Golem>

⁸<http://www.hs.uni-hamburg.de/Lofar>

⁹<http://www.harrisgeospatial.com>

4. Framework

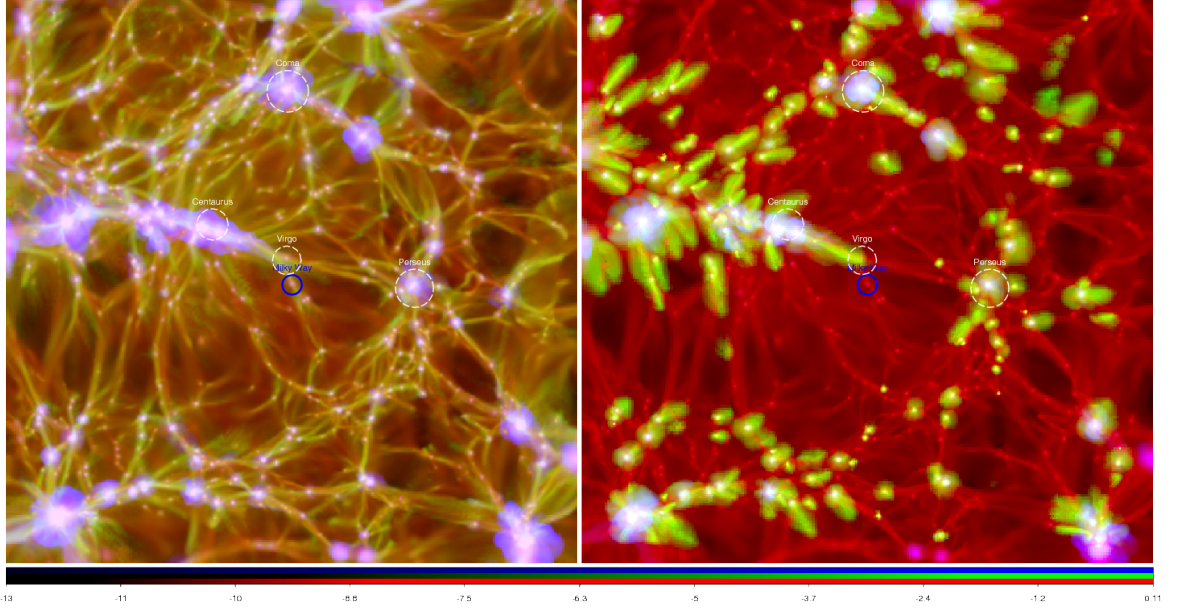


Figure 4.3: Slice of the simulated volume in the CS for the *primordial* (left) and the *astrophysical* model (right). Shown is an overlay of the gas density (red), the temperature (blue) and magnetic fields (green).

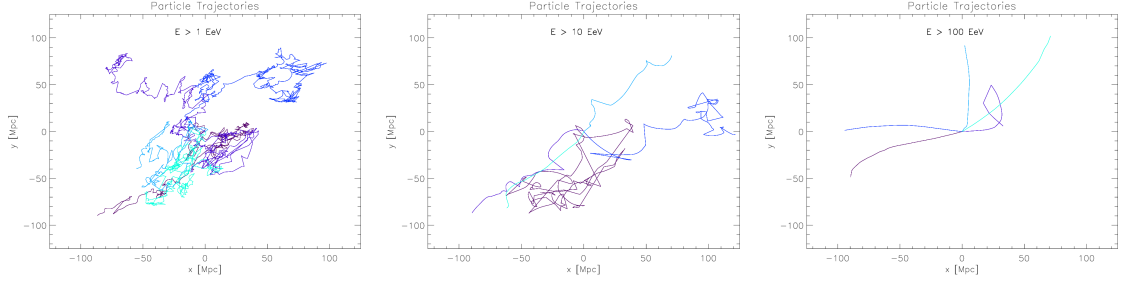


Figure 4.4: Simulated path of propagation of five UHECR protons with final energy of 1 , 10 and 100 EeV (left to right) in the *primordial* model. Every color refers to a different particle.

suit to investigate how these fields contribute to the overall deflection of UHECRs.

Fig. 4.3 shows a slice of the simulated volume in the CS. The distribution of gas and temperature are the same in both models, we indicate the position of the Virgo, Coma, Perseus and Centaurus clusters as well as the position of the MW¹⁰. Magnetic fields on the other hand permeate the whole volume in the *primordial* model (left), while in the *astrophysical* model (right) fields are concentrated in the regions of high gas density.

In Fig. 4.4 we present the path of propagation of UHECR protons injected at different energies in the centre of the *primordial* model. At the lowest energies, ~ 1 EeV, particles

¹⁰We comment that in our simulations the difference between the real positions of the above clusters and the simulated ones is of the order of a couple of ~ 5 Mpc at most (and up to ~ 5 Mpc limited to the case of the Perseus cluster). These differences are ascribed to numerical effects (i.e. a different resolution in the code used to generate the initial conditions and in the code used to produce our MHD simulations), but do not pose particular problems for the statistical analysis we perform here.

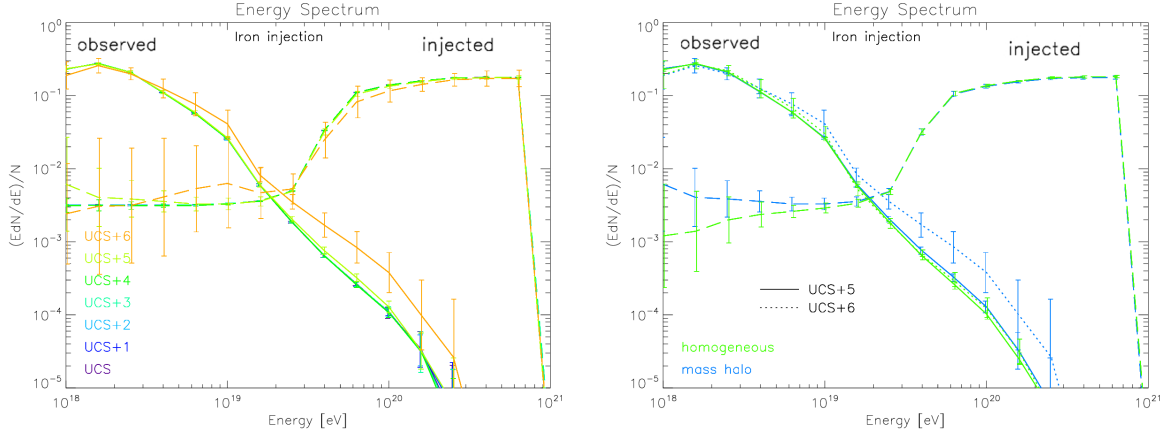


Figure 5.1: Normalized energy spectrum of UHECRs as injected at all sources (dashed) and recieved by the observer (solid) in the UCS in a pure iron injection scenario.

propagate diffusively and lose information about the position of their source on rather short distances. At intermediate energies, ~ 10 EeV, particles propagate on much straighter lines, still they lose information about their source within a few Mpc. At the highest energies, ~ 100 EeV, propagation has become more ballistic and particles are deflected by only a few degrees over 100 Mpc. This raises hope for the possibility of UHECR astronomy at the highest energies.

5. Results and Discussion

5.1. Energy Spectrum

In Fig. 5.1 we show the number of received particles as function of their observed (solid) and injected energy (dashed) in the UCS. The energy spectra were normalized with the total number of observed particles and multiplied by E , the inverse energy dependence of the injected spectrum, for better comparison and to highlight the differences. The injected spectrum increases sharply around 20 – 60 EeV. This is due to photo-disintegration of injected high energy iron nuclei that can produce a number of light remnant nuclei at lower energies $\sim E/A$. Several of these can be measured by a magnetized observer (cf. Sec. 4.2) and account for most of the particles observed with $E \lesssim 10^{19}$ eV. In computation of the plot we count energies of all measured particles at moment of observation and injection. If several remnants of the same injected particle are measured, that injection energy is double-counted.

In the left panel of Fig. 5.1 we can see that all the magnetic field models allowed by the upper limits from the CMB (UCS+5 and below) are in good agreement with each other. They all show a low cosmic variance since for source densities above 10^{-4} Mpc^{-3} (Abreu et al. 2013) the average distance between sources is much shorter than the characteristic propagation length of UHECRs, according to the propagation theorem (e. g. Aloisio and Berezhinsky 2004). Only the strongest magnetic field model UCS+6 shows a harder spectrum as well as an increased cosmic variance above $2 \cdot 10^{19}$ eV. In the right panel we compare in the strongest models the

5. Results and Discussion

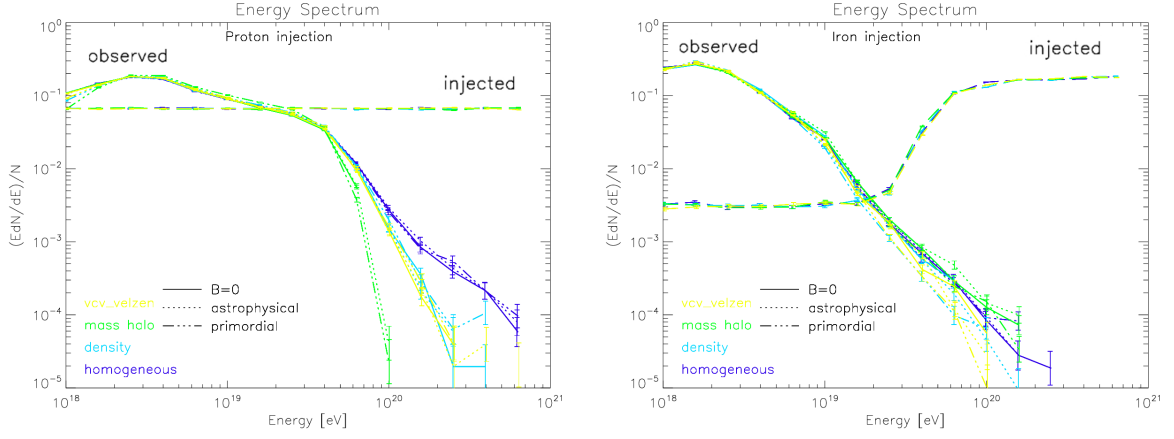


Figure 5.2: Same as Fig. 5.1 in the CS in pure proton (left) and pure iron (right) injection scenarios.

case of *mass halo* injection (blue, same as shown in the left panel) to *homogeneous* injection (green). We can see that the increase is only present for discrete sources at *mass halos* and hence strongly depends on the distribution of sources.

More particles from nearby sources are allowed to reach the observer in an environment with stronger magnetic fields (cf. Sec. 5.3). In the UCS+6 fields are strong enough to increase the number of observed events from nearby sources at the highest observed energies (cf. Fig. 5.6). The exact distribution of nearby sources, or better, their number and distance to the observer determines the exact slope of the spectrum at the highest energies; more sources at a low distance cause a harder spectrum and increase the maximum energy of arriving particles. As pointed out in Sec. 4.3, the UCS+6 violates the constraints given by observation of anisotropies in the CMB (Ade et al. 2015). Therefore EGMFs with strength in agreement with present constraints from observations are not expected to significantly influence the observed energy spectrum.

Fig. 5.2 shows the energy spectrum of UHECRs in the CS. Comparison between pure proton (left) and pure iron injection (right) shows that the spectrum is softer in the iron injection case. While injection of hydrogen with 1000 EeV allows for observation of UHECR events with several hundred EeV, the upper limit is much lower for iron. The same trend can be found in the UCS when comparing the iron injection in Fig. 5.1 to the case of proton injection presented in Hackstein et al. (2016). The reason for the decreased upper limit and the softer spectrum at high energies, $> 20 \text{ EeV} \approx E_{\text{max}}/A$, is the shorter energy loss length of heavier nuclei and their additional loss of energy through disintegration. The latter accounts for the softer spectrum at lower energy, where most of the particles are remnants of heavy nuclei injected at higher energies.

5. Results and Discussion

In the pure proton injection scenario the sharpness of the GZK-cut-off $\gtrsim 4 \cdot 10^{19}$ eV strongly depends on the set of sources. In contrast, for the pure iron injection case all the spectra are in agreement with one another. This is due to the low number of particles at that energy in the iron injection scenarios of the CS, where we find less than 100 particles above the GZK-limit at $\sim 4 \cdot 10^{19}$ eV. In 5.3 is shown the very same plot for scenarios, where we only considered UHECRs with $E > 20$ EeV in order to gain more decent number statistics in feasible computation time. For better number statistics the distribution of sources influences the shape of the energy spectrum at the highest energies, even for a heavy injection component. No significant influence of the magnetic field can be seen in any of the energy spectra in the CS.

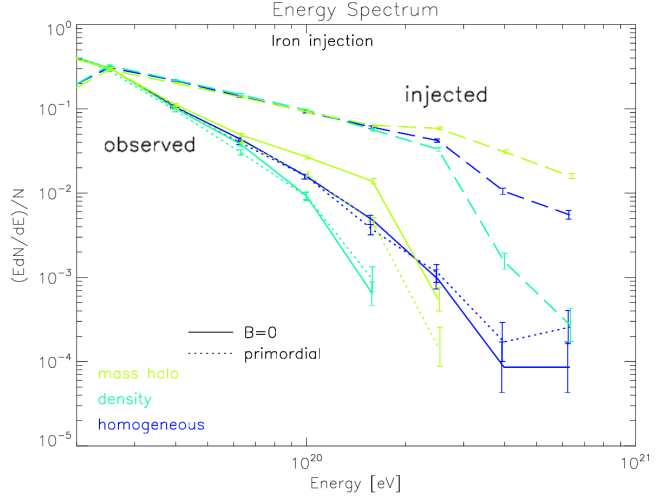


Figure 5.3: Same as Fig. 5.1 for particles above 10 EeV in the $B=0$ model and several injection scenarios of the CS. The error bars show the Poissonian noise for the single observer

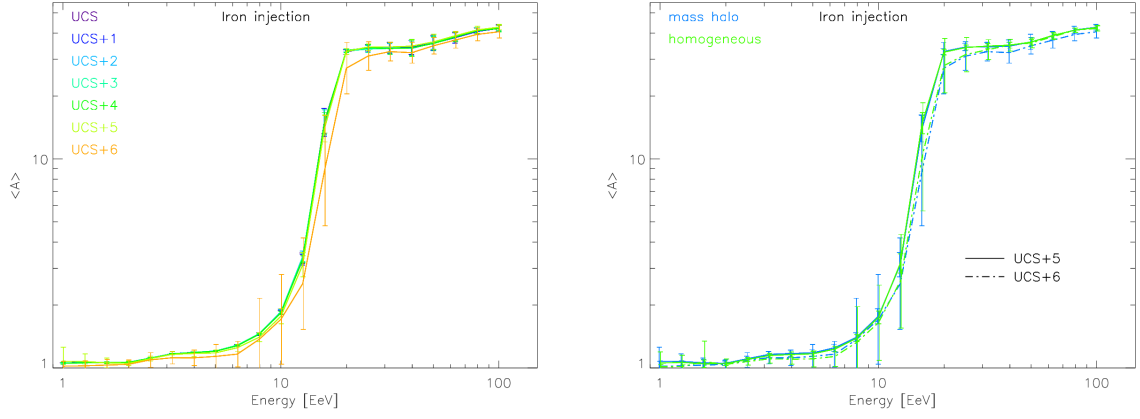


Figure 5.4: Average number of nucleons A of UHECRs as a function of energy as received by the observers in the UCS in scenarios with pure iron *mass halo* (left and right, blue) and *homogeneous* injection (right, green). The error bars show the 1σ standard deviation for the 18 observers.

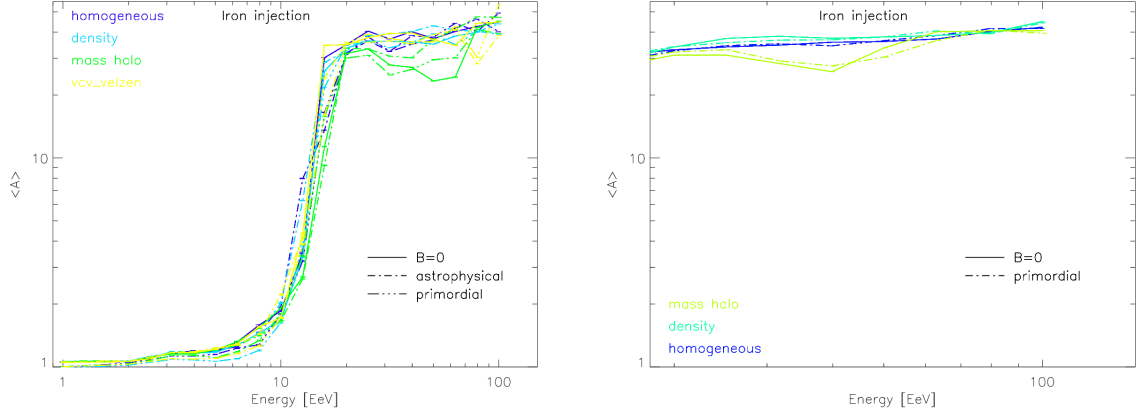


Figure 5.5: Same as Fig. 5.4 in the several injection scenarios of the CS. Left: comparison of the several magnetic field models. Right: particles above 10 EeV in the $B=0$ model. The error bars show the standard error for the single observer.

5.2. Composition

In Fig. 5.4 we present the average number of nucleons $\langle A \rangle$ of received UHECR nuclei as function of their energy. There is a strong increase in $\langle A \rangle$ that starts smoothly at a few EeV and ends abruptly at $\sim 20 \text{ EeV} \approx E_{\text{max}}/A_{\text{Fe}}$. We see that this coincides with the energy expected for a proton that broke away from an iron nucleus injected at the maximum energy of $E_{\text{max}} = 1000 \text{ EeV}$. A single iron nucleus can dissolve into $A_{\text{Fe}} = 56$ protons that can all be observed by a magnetized observer. Therefore the amount of light nuclei increases drastically at lower energies and reduces $\langle A \rangle$.

At higher energies, only heavy nuclei are observed, those that may have emitted a few of their nucleons already together with a fraction of their initial energy. The higher the energy, the less nucleons are likely to have been emitted and hence $\langle A \rangle$ increases slowly. The lack of protons at high energies from a purely heavy injection composition together with the report

5. Results and Discussion

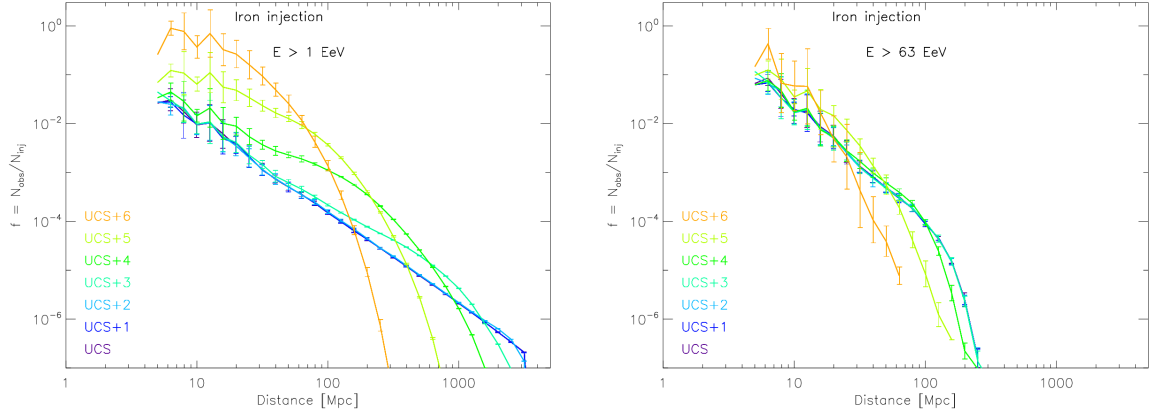


Figure 5.6: Ratio of observed to injected number of particles per source as function of distance to the observer in the UCS in a pure iron injection scenario. We consider all particles above the displayed limit. We take the average over all 18 observers, the error bars show the 1σ standard deviation.

of dominantly light nuclei at the highest energies by TA (Abbasi et al. 2015) would therefore imply the injection of light nuclei at the highest energies.

The shape of the presented plot is determined by the initial composition, energy spectrum and maximum energy of UHECRs. It can be used to gain information about the sources. We exemplary investigate this realization to see whether magnetic fields and source distribution significantly influence the observed composition of UHECRs.

The observed composition in the UCS (Fig. 5.4, left) shows well agreement for the weak magnetic field models (UCS+4 and below). For stronger magnetic fields the average value of $\langle A \rangle$ decreases slightly at all energies due to extended travel time and hence larger probability for disintegration (cf. e. g. Bertone et al. 2002; Globus, Allard, and Parizot 2008). Further, the cosmic variance increases, especially below 10 EeV; the well agreement between *homogeneous* and *mass halo* injection (right panel) indicates that this is independent of the sources but reflects the importance of the local distribution of magnetic field around the observer. Strong magnetic fields close to the observer can attract heavy nuclei at low energy and thus effectively increase $\langle A \rangle$.

In the CS (Fig. 5.5) the pervasive field of the *primordial* model reduces $\langle A \rangle$ at energies below 10 EeV. Here the standard error shows the statistical uncertainty of this measure, which is much less than cosmic variance shown for the UCS. In case that the strengths of EGMFs are right below the upper limits there is a good chance to see an imprint of our cosmic realization of EGMFs in $\langle A \rangle$.

5.3. Source Contribution

We call $f = N_{\text{obs}}/N_{\text{inj}}$ the ratio of the number of observed particles N_{obs} that originated from a single source to the total number of particles that were injected by that source N_{inj} . Besides the quadratic decrease due to geometric diffusion on a sphere it is a complicated function of distance that is influenced by all interactions UHECRs experience during propagation: energy loss, decay as well as deflection by magnetic fields.

In Fig. 5.6 you can see f as a function of distance to the source. At low energies (left panel) and distances above a few tens of Mpc the weakest magnetic field models in the UCS show the expected quadratic decrease in f . Below that, f increases slightly faster with decreasing distance. This is simply because the injected high energy iron nuclei dissolve into a shower of remnant particles with only narrow diffusion due to the high Lorentz factor. If injected at rather low distance, several of these remnants may hit a finite observer sphere (cf. Sec. 4.3) and thus artificially increase the number of observed particles from very nearby sources. It is worth to note that though in a magnetic field free case an ideal point-like observer could receive only one of the remnants of a single injected particle, magnetic fields deflect the remnants such that several of them may reach a magnetized observer.

The longest possible distance to a source from which we can receive particles is given by the lifetime of the universe, the so called particle horizon at $d_{\text{pH}} \sim 14$ Gpc, and demands $f(d > d_{\text{pH}}) = 0$. To save unnecessary computation time (cf. Sec. 4.3) the maximum travel distance of particles in the simulation was set to 4 Gpc, where we find $f = 0$ for the very weak fields in the UCS in Fig. 5.6. Stronger mag-

netic fields bend the path of propagation of charged particles and thereby increase the travelled distance. Particles from far away sources cannot reach the observer within the lifetime of the universe (cf. Fig. 5.7). This defines a magnetic horizon $< d_{\text{pH}}$ beyond which sources are invisible in the UHECR sky, as discussed e. g. in Kotera and Lemoine (2008) or Alves Batista and Sigl (2014). The latter concluded that suppression of the flux is expected at energies below $\sim 10^{17}$ eV. At higher energies the suppression of the flux from far away sources is compensated by the amplification of the flux from nearby sources (e. g. Sigl, Miniati, and Enßlin 2004 and Globus, Allard, and Parizot 2008).

When traversing a volume, a particle is detected by an observer when it passes at a distance less than the size of the observer. The probability of detection is then proportional to

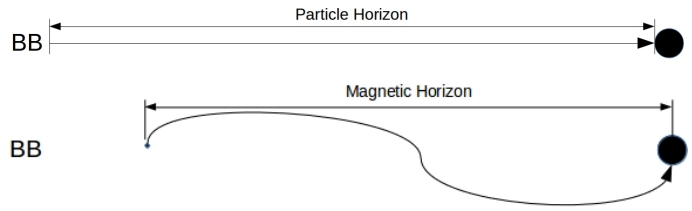


Figure 5.7: Longest possible travelled distance of a charged particle in the lifetime of the universe in absence of magnetic fields (top) and under constant deflection (bottom).

5. Results and Discussion

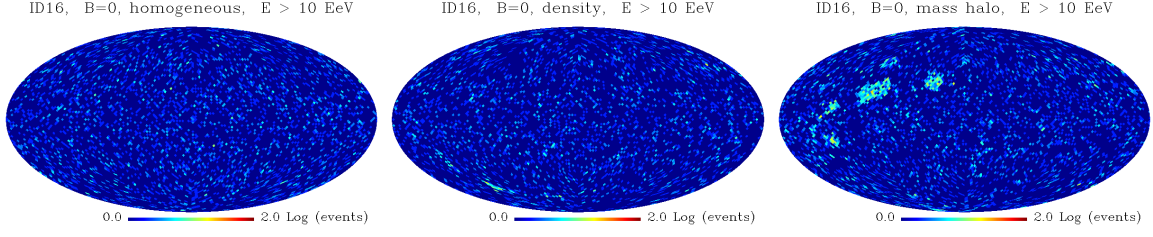


Figure 5.8: full-sky maps of arrival directions in the $B=0$ model for injection from *homogeneous* (left), *density* (center) and *mass halo* sources (right). All maps are shown for a minimum energy of 10 EeV of events.

the length d of the particle trajectory. As pointed out in Sec. 2.3, for a charged particle that is deflected by magnetic fields, d increases and hence does the probability of detection. Indeed, in Fig. 5.6 f increases with the strength of the magnetic field and further, with the distance, until sources are beyond the magnetic horizon.

UHECR nuclei might even get trapped in a loop in a sufficiently strong and extended EGMF. In our simulation such a particle is measured every time it enters the observer sphere and thus produces a strong excess in the full-sky of event numbers. This is the case in the stronger magnetic field models (UCS+3 and above). Though in reality a single particle can be measured only once, this reflects the highly increased chance for particles to hit an observer embedded in a strong and extended magnetic structure. It is necessary to check case by case whether the resulting anisotropy is to be considered artificial or not. If the magnetic structure is e. g. extended in two dimensions, but narrow in the third, this would favour arrival directions in the plane due to a higher probability of presence inside that structure.

For much faster UHECRs, energy losses are more severe and we see in the right panel of Fig. 5.6 that f decreases faster than with the square of distance. The energy loss length of these nuclei is much shorter than the particle horizon, which further reduces the maximum distance to sources visible in the UHECR sky at higher energy.

While the statistical noise obviously increases with increasing distance, the cosmic variance of f is the strongest at lower distances. This is because there are fewer sources in a lower distance bin to determine the value of f for a single observer and hence small differences in the source distance have a stronger relative impact. For both energy limits, the cosmic variance increases with increasing magnetic field strength over all distances.

5.4. Harmonic Analysis

In this section we present the angular power C_l of the full-sky of arrival directions. It is obtained by decomposing the full-sky of events in spherical harmonics and then combine the coefficients of equal multipoles, for more details on the calculation see e. g. Tinyakov and Urban (2015). In Fig. 5.8 we present full-sky maps of arrival directions for different distribution of sources.

5. Results and Discussion

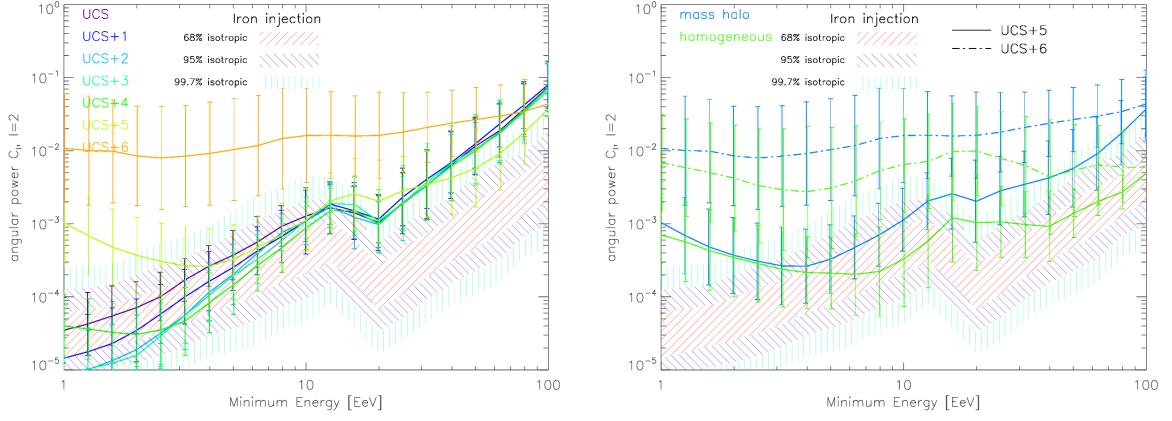


Figure 5.9: Average angular power C_l as a function of minimum energy of observed UHECRs in the UCS in a pure iron injection scenario. The left plot compares different strength of EGMFs in a mass halo injection scenario, while the right plot compares mass halo to homogeneous injection in the strongest EGMF models. The shaded regions show the $1 - 3\sigma$ isotropic prediction.

The isotropic prediction shows the $1 - 3\sigma$ standard deviation of 125 observers in a $B=0$ *homogeneous* injection scenario with otherwise unaltered parameters. This choice does not result in the most isotropic prediction since it equally generates all the artificial contributions to the anisotropy that are caused by the setting of the simulation, e. g. finite observer effect, over-count of secondary nuclei and periodicity. On the other hand, this makes the presented prediction the best choice to find the qualitative contribution of source distribution and magnetic fields.

The angular power C_l of the quadrupole $l = 2$ is shown in Fig. 5.9 as a function of minimum energy of considered particles for a pure iron injection in the UCS. Below 20 EeV there is a general increase in anisotropy in all simulations. At that energy the remnants of the most rapid heavy nuclei account for most of the observed events (cf. Sec. 5.1). As discussed in Sec. 4.2, there is an artificial increase in the number of observed remnants that point to nearby sources.

The left panel of Fig. 5.9 shows that the weaker magnetic field models (UCS+4 and below) in the *mass halo* injection scenarios are in good agreement over all energies. At the highest energies many observers show an excess from isotropy mirroring the anisotropic distribution of nearby sources within the GZK-horizon, as has been shown already for the case of pure proton injection in Hackstein et al. (2016) (also cf. e. g. Harari, Mollerach, and Roulet 2014). For stronger magnetic fields (UCS+5), an anisotropic signal forms at low energy and in the strongest model (UCS+6) the signal is present over all energies. This signal is built up mostly by particles that are trapped in a loop in an extended and strong magnetic field structure and hit the observer repeatedly with similar arrival directions.

5. Results and Discussion

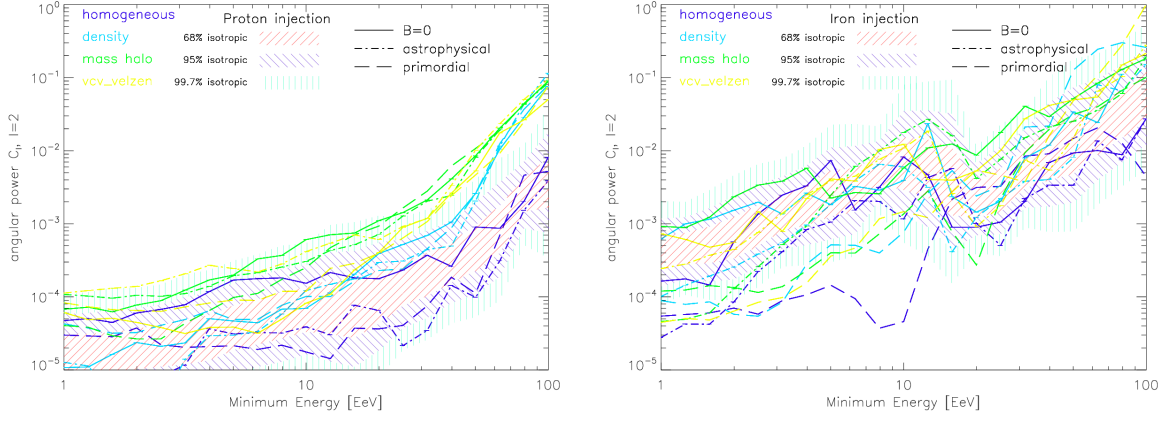


Figure 5.10: Same as Fig. 5.9 in the CS in pure proton (left) and pure iron (right) injection scenarios.

In the right panel of Fig. 5.9 we compare *mass halo* to *homogeneous* injection in the two strongest UCS models. The anisotropy is increased in the *homogeneous* case similar to the *mass halo* case, which shows that this effect is independent of sources, but can be boosted by a suitable source distribution. The big cosmic variance on the anisotropic signal indicates that it depends strongly on the distribution of magnetic fields in the near vicinity of the observer. No such anisotropy has been observed at the EeV scale (e. g. Pierre Auger Collaboration 2012). This leads to the conclusion that there is no such strong and extended magnetic field structure in the vicinity of the MW that could account for such an effect.

In Fig. 5.10 we show the quadrupole moment of the angular power C_l for several injection scenarios in the different magnetic field models of the CS. For the proton injection scenarios (left panel) the influence of the source distribution at the highest energies is clearly visible: all injection scenarios that follow the large scale structure, namely *density*, *mass halo* and *vcv_velzen*, show the same anisotropic quadrupole signal at 100 EeV. For *homogeneous* injection the graphs are in agreement with the isotropic prediction. At slightly lower energies ($\gtrsim 40$ EeV) the slope of the energy dependence of C_l differs slightly between the injection scenarios. At even lower energies all the graphs are in agreement with the isotropic prediction, only the *mass halo* scenarios tend to the upper end of the prediction. This is due to the high number of sources in the near vicinity of the observer. While a uniform source distribution would suggest less than one source within 10 Mpc distance, there are more than 10 in the *mass halo* catalogue.

6. Conclusion

The right panel of Fig. 5.10 shows the pure iron injection scenarios in the different magnetic field models of the CS. All scenarios are in good agreement with the isotropic prediction, only at the very highest energies the trend goes to the upper boarder of the prediction for injection scenarios following the LSS, *density*, *mass halo* and *vcv_velzen*. Indeed, in Fig. 5.10, where we have greater number statistics at the highest energies in the iron injection scenarios in the CS, we can see that the *homogeneous* injection results in a much weaker quadrupole at the highest energies. We see in the right panel of Fig. 5.10 at the transition from heavy to light composition at around 10 EeV that the increase in anisotropy due to observation of multiple remnant particles is washed out in the *primordial* magnetic field model. In the CS we see no additional anisotropy in the strongly magnetized model but only the tendency to wash out the anisotropic signal.

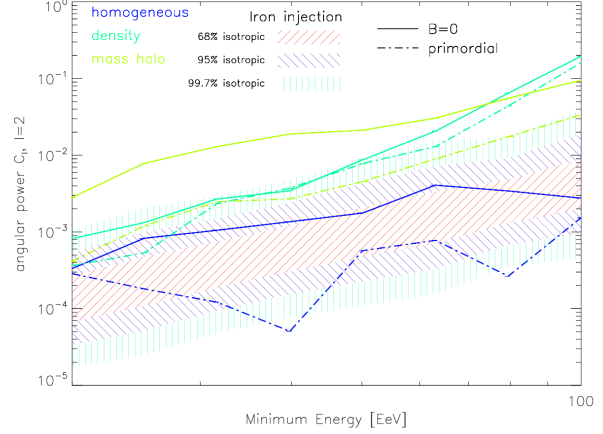


Figure 5.11: Same as Fig. 5.10 in the $B=0$ model (more are on the way) and several injection scenarios of the CS.

6. Conclusion

This thesis presents an investigation on the propagation of UHECRs in an extended set of MHD-simulations of cosmic volumes. We have probed a set of unconstrained simulations of the Universe where we investigate different magnetic field strengths of primordial magnetic fields. We further explored constrained simulations of our local Universe, where for the first time we made use of the initial conditions obtained in Sorce et al. (2016) with ENZO and magneto-hydrodynamics. In this simulation we tested several models for magnetogenesis, namely primordial versus astrophysical seeding processes.

A key point of our investigation is to assess the impact of the variation of a number of parameters on the observables of UHECRs, namely on their energy spectrum, composition and anisotropies in the arrival directions. We varied the number of and distance to sources of UHECRs with use of discrete position catalogues for steady sources or continuous distribution function equal to the gas density to realize transient sources. We further investigated a range of field strengths in voids as well as different seeding processes of extra-galactic magnetic fields. These variations have been probed with injection of a pure proton composition as well as with a pure iron composition in order to investigate the consequences of the additional effects in the propagation of heavy nuclei. The results of that investigation have been summarized in Tab. 3.

6. Conclusion

Observable \ Component	nearby Sources	Strong CMFs	Heavier Composition
spectrum	determine E_{\max} & slope $> E_{\text{GZK}}$	\times	softer spectrum
anisotropy	imprint at highest E	favour directions wash out	stronger deflection
observed composition	\times	\times	(<i>obvious</i>)

Table 3: Overview on the results of this thesis. First column: observable that is influenced. Second column: impact of choice of sources. Third column: influence of strong CMFs. Fourth column: implications of a heavier injection component. **Blue** comments are only on the UCS, **green** comments on the CS, black concern both.

To summarise, our results suggest a) regardless of the distribution of sources, a magnetization in voids of a few nG can produce an anisotropic distribution of UHECRs at a few EeV that is in conflict with measurements. For even stronger fields, anisotropy can be found at all energies below 100 EeV; b) at the highest energies, ~ 100 EeV, the distribution of sources determines the departure from the isotropic case. Extragalactic magnetic fields within observational limits do not alter this feature.

Sources

Energy Spectrum We have found that the distribution of sources does not affect the observed energy spectrum of UHECRs, as predicted by the propagation theorem (e. g. Aloisio and Berezhinsky 2004). Only at energies above the GZK-limit of $\sim 4 \cdot 10^{19}$ eV the **slope of the spectrum** depends on the distribution of the most nearby sources; the distance to the nearest source determines the **end of the energy spectrum** (Globus, Allard, and Parizot 2008).

Arrival Directions At energies $\lesssim 10^{19}$ eV the arrival directions of events are generally not affected by the distribution of sources, since the majority of particles originate far away (> 1 Gpc, cf. e. g. Sigl, Miniati, and Enßlin 2004). On the other hand, the distribution of most nearby sources leaves an **imprint at the highest energies** ($\lesssim 10^{20}$ eV), even in the strongest magnetic field models and regardless of source density (cf. e. g. Harari, Mollerach, and Roulet 2014).

Composition Very **small variance** is found for the observed composition of UHECRs in all of the models (cf. e. g. Globus, Allard, and Parizot 2008).

Magnetic fields

Energy Spectrum In our investigation, extragalactic magnetic fields in agreement with present observational limits do **not affect the propagated energy spectrum**. Only magnetic fields that exceed those limits can cause a harder spectrum (Globus, Allard, and Parizot 2008).

Arrival Directions Magnetic fields showed diversified effects on anisotropy in the arrival direction in the different tested models. In the constrained simulation the magnetic fields of astrophysical origin show negligible effects on the arrival directions. On the other hand, magnetic fields with primordial origin cause diffusive propagation and delete (“**wash out**”) information on the direction to their sources on rather short length scales and thus produce a isotropic distribution of arrival directions (cf. e. g. Takami, Inoue, and Yamamoto 2012).

In the unconstrained simulation, strong magnetic fields can **create an anisotropic picture** in most of the observer skies. The charged particles are forced to move in widely extended loops and thus favour directions in plane of the loop.

Composition In a stronger magnetic field charged particles effectively travel longer distance. This grants more time to disintegration processes and result in a **lighter spectrum** (cf. e. g. Globus, Allard, and Parizot 2008). Significant effects could only be found for strong magnetic fields in voids right below the allowed limit of \sim nG; strong magnetic fields around the observer can amplify this effect.

Composition

Energy Spectrum A heavier injected component has a shorter energy loss length and thus the observed energy **spectrum is softer**. In addition, their remnants account for a major part of the low energy particles, which further softens the spectrum (cf. e. g. Allard 2012).

Arrival Directions The magnetic rigidity decreases with increasing charge, therefore heavy particles undergo stronger deflection in magnetic fields. Visible effects of that can be seen in the distribution of arrival directions, where the reported **effects are more prominent** for a heavier injection component.

Composition In course of this thesis we did not investigate the implications of the injected particle species on the observed composition of UHECRs, more details on that can be found e. g. in Abbasi et al.; Arisaka et al. (2005; 2007) or Taylor (2014).

In this work we have varied a number of parameters on the sources of UHECRs and on cosmic magnetic fields; we arranged an overview on the effects on observables of UHECR measurement. Most of the effects are independent of other variations and are well described in the literature. We found diversified effects of extragalactic magnetic fields on the anisotropy that strongly depend on the actual distribution of fields around the observer.

7. Acknowledgement

In the unconstrained simulation, strongly magnetized regions around the observer can create anisotropic patterns in arrival directions of UHECRs below the GZK-limit. Such patterns are not observed in real observations and can be used to discard models of magnetogenesis.

In the constrained simulation, magnetic fields of astrophysical origin showed no significant effects at all, owing to their rather small volume filling fraction. On the other hand, strong magnetic fields from primordial seeding only showed the tendency to lower anisotropy which is measured in the absence of those fields. Due to the high uncertainty in the actual shape of magnetic fields in the local Universe, a single constrained simulation can never cover all possible scenarios that are in agreement with observation. The analysis of a diversified set of constrained simulations is necessary to see whether some of these scenarios can be ruled out by UHECR observation. The rather coarse dark matter resolution of the constrained initial conditions tested here may have prevented the formation of dwarf galaxies in voids, and therefore their additional possible magnetisation effect in voids is underestimated here. With future re-simulations we will try to cure for this potential limitation in our astrophysical scenario.

In this thesis we neglected additional deflection by the galactic magnetic field of the Milky Way, which is expected to be rather low due to quasi rectilinear propagation of UHECRs at energies concerned in this thesis. The comparably short time necessary to transit the Milky Way does not allow significant changes on the energy spectrum or the composition either.

Our analysis shows that UHECR astronomy probably is possible at the highest energies, since cosmic magnetic fields within present observational limits cause only small deflections. The completion of the northern part of the Pierre Auger Observatory and the following full sky coverage of UHECR measurement will allow to measure sufficient number of those particles in the coming decades and finally finish the search for the most energetic accelerators in our Universe. Beyond that, the improved anisotropy measurements promise to bear the opportunity to constrain magnetic field seeding processes.

7. Acknowledgement

First, I would like to thank Marcus Brüggen for providing me with the very interesting topic of this thesis. Furthermore I would like to thank my dedicated supervisor Franco Vazza for his unstinting support throughout the whole thesis. Finally, my thanks go to my family and to Nadine for private support.

Additionally the whole group would like to thank G. Sigl and A. Dundovic for their precious scientific support and fruitful discussions, as well as all the other developers of CRPropa for making the code publicly available. We also acknowledge the usage of computational resources of the CHRONOS Call 2014 at CSCS (Lugano, Switzerland) and at the Jülich Su-

percomputing Center (JSC) under project number 7006, as well as the use of resources of the Golem and Lofar Clusters at Hamburger Sternwarte.

References

- Abbasi, R. U. et al. (2005). “A Study of the Composition of Ultra-High-Energy Cosmic Rays Using the High-Resolution Fly’s Eye”. In: *The Astrophysical Journal* 622.2, p. 910. URL: <http://stacks.iop.org/0004-637X/622/i=2/a=910>.
- Abbasi, R. U. et al. (2008). “First observation of the Greisen-Zatsepin-Kuzmin suppression”. In: *Phys. Rev. Lett.* 100, p. 101101. DOI: 10.1103/PhysRevLett.100.101101. arXiv: astro-ph/0703099 [astro-ph].
- Abbasi, R. U. et al. (2015). “Study of Ultra-High Energy Cosmic Ray composition using Telescope Array’s Middle Drum detector and surface array in hybrid mode”. In: *Astroparticle Physics* 64, pp. 49–62. DOI: 10.1016/j.astropartphys.2014.11.004. arXiv: 1408.1726 [astro-ph.HE].
- Abbasi, R. et al. (2016). “Report of the Working Group on the Composition of Ultra High Energy Cosmic Rays”. In: *Proceedings of International Symposium for Ultra-High Energy Cosmic Rays (UHECR2014)*, id.010016, <NUMPAGES>7</NUMPAGES> pp. P. 010016. DOI: 10.7566/JPSCP.9.010016. arXiv: 1503.07540 [astro-ph.HE].
- Abraham, J. et al. (2008). “Observation of the suppression of the flux of cosmic rays above 4×10^{19} eV”. In: *Phys. Rev. Lett.* 101, p. 061101. DOI: 10.1103/PhysRevLett.101.061101. arXiv: 0806.4302 [astro-ph].
- Abreu, Pedro et al. (2013). “Bounds on the density of sources of ultra-high energy cosmic rays from the Pierre Auger Observatory”. In: *JCAP* 1305.05, p. 009. DOI: 10.1088/1475-7516/2013/05/009. arXiv: 1305.1576 [astro-ph.HE].
- Ade, P. A. R. et al. (2015). “Planck 2015 results. XIX. Constraints on primordial magnetic fields”. In: arXiv: 1502.01594 [astro-ph.CO].
- Allard, D. (2012). “Extragalactic propagation of ultrahigh energy cosmic-rays”. In: *Astroparticle Physics* 39, pp. 33–43. DOI: 10.1016/j.astropartphys.2011.10.011. arXiv: 1111.3290 [astro-ph.HE].
- Aloisio, R. and V. Berezhinsky (2004). “Diffusive Propagation of Ultra-High-Energy Cosmic Rays and the Propagation Theorem”. In: *ApJ* 612, pp. 900–913. DOI: 10.1086/421869. eprint: astro-ph/0403095.
- Alves Batista, R. and G. Sigl (2014). “Magnetic horizons of ultra-high energy cosmic rays”. In: *ArXiv e-prints*. arXiv: 1410.7800 [astro-ph.HE].
- Alves Batista, R. et al. (2015). “Effects of uncertainties in simulations of extragalactic UHECR propagation, using CRPropa and SimProp”. In: *JCAP* 1510.10, p. 063. DOI: 10.1088/1475-7516/2015/10/063. arXiv: 1508.01824 [astro-ph.HE].
- Anderson, Carl D. (1932). “THE APPARENT EXISTENCE OF EASILY DEFLECTABLE POSITIVES”. In: *Science* 76.1967, pp. 238–239. ISSN: 0036-8075. DOI: 10.1126/science.

References

- 76.1967.238. eprint: <http://science.sciencemag.org/content/76/1967/238.full.pdf>. URL: <http://science.sciencemag.org/content/76/1967/238>.
- Arisaka, Katsushi et al. (2007). “Composition of UHECR and the Pierre Auger Observatory spectrum”. In: *Journal of Cosmology and Astroparticle Physics* 2007.12, p. 002. URL: <http://stacks.iop.org/1475-7516/2007/i=12/a=002>.
- Armengaud, Eric, Guenter Sigl, and Francesco Miniati (2005). “Ultrahigh energy nuclei propagation in a structured, magnetized Universe”. In: *Phys. Rev. D* 72, p. 043009. DOI: 10.1103/PhysRevD.72.043009. arXiv: astro-ph/0412525 [astro-ph].
- Armengaud, Eric et al. (2007). “Crpropa: a numerical tool for the propagation of uhe cosmic rays, gamma-rays and neutrinos”. In: *Astropart. Phys.* 28, pp. 463–471. DOI: 10.1016/j.astropartphys.2007.09.004. arXiv: astro-ph/0603675 [astro-ph].
- Batista, Rafael Alves et al. (2016). “CRPropa 3 - a public astrophysical simulation framework for propagating extraterrestrial ultra-high energy particles”. In: *Journal of Cosmology and Astroparticle Physics* 2016.05, p. 038. URL: <http://stacks.iop.org/1475-7516/2016/i=05/a=038>.
- Bertone, G. et al. (2002). “Ultrahigh energy heavy nuclei propagation in extragalactic magnetic fields”. In: *Physical Review Letters* 66.10, 103003, p. 103003. DOI: 10.1103/PhysRevD.66.103003. eprint: astro-ph/0209192.
- Bertone, Gianfranco et al. (2002). “Ultrahigh energy heavy nuclei propagation in extragalactic magnetic fields”. In: *Phys. Rev. D* 66 (10), p. 103003. DOI: 10.1103/PhysRevD.66.103003. URL: <http://link.aps.org/doi/10.1103/PhysRevD.66.103003>.
- Bertone, Serena, Corina Vogt, and Torsten Ensslin (2006). “Magnetic Field Seeding by Galactic Winds”. In: *Mon. Not. Roy. Astron. Soc.* 370, pp. 319–330. DOI: 10.1111/j.1365-2966.2006.10474.x. arXiv: astro-ph/0604462 [astro-ph].
- Bhattacharjee, P. (2000). “Origin and propagation of extremely high energy cosmic rays”. In: *Physical Reports* 327, pp. 109–247. DOI: 10.1016/S0370-1573(99)00101-5. eprint: astro-ph/9811011.
- Blasi, P. (2013). “The origin of galactic cosmic rays”. In: *The Astronomy and Astrophysics Review* 21, 70, p. 70. DOI: 10.1007/s00159-013-0070-7. arXiv: 1311.7346 [astro-ph.HE].
- Bowman, Kenneth P. (2005). *An Introduction to Programming with IDL: Interactive Data Language*. Academic Press. ISBN: 012088559X. URL: <http://www.worldcat.org/isbn/012088559X>.
- Bryan, G. L. et al. (2014). “ENZO: An Adaptive Mesh Refinement Code for Astrophysics”. In: *ApJS* 211, 19, p. 19. DOI: 10.1088/0067-0049/211/2/19. arXiv: 1307.2265 [astro-ph.IM].
- Cen, R. and J. P. Ostriker (1992). “Galaxy formation and physical bias”. In: *ApJL* 399, pp. L113–L116. DOI: 10.1086/186620.
- Dedner, A. et al. (2002). “Hyperbolic Divergence Cleaning for the MHD Equations”. In: *Journal of Computational Physics* 175.2, pp. 645–673. ISSN: 0021-9991. DOI: <http://dx.doi.org/10.1006/jcp.2002.3333>.

References

- org/10.1006/jcph.2001.6961. URL: <http://www.sciencedirect.com/science/article/pii/S002199910196961X>.
- Donnert, J. et al. (2009). “Cluster Magnetic Fields from Galactic Outflows”. In: *Mon. Not. Roy. Astron. Soc.* 392, pp. 1008–1021. DOI: 10.1111/j.1365-2966.2008.14132.x. arXiv: 0808.0919 [astro-ph].
- Dova, M. T. (2016). “Ultra-High Energy Cosmic Rays”. In: *ArXiv e-prints*. arXiv: 1604.07584 [astro-ph.HE].
- Epele, L. N. and E. Roulet (1998). “On the propagation of the highest energy cosmic ray nuclei”. In: *Journal of High Energy Physics* 10, 009, p. 009. DOI: 10.1088/1126-6708/1998/10/009. eprint: astro-ph/9808104.
- F. Hess, V. (1912). “Über Beobachtungen der durchdringenden Strahlung bei sieben Freiballonfahrten”. In: *Physikalische Zeitschrift* 13, pp. 1084–1091.
- Fang, Ke and Kumiko Kotera (2016). “The Highest-Energy Cosmic Rays Cannot be Dominantly Protons from Steady Sources”. In: *Astrophys. J.* 832.1, p. L17. DOI: 10.3847/2041-8205/832/1/L17. arXiv: 1610.08055 [astro-ph.HE].
- Globus, N., D. Allard, and E. Parizot (2008). “Propagation of high-energy cosmic rays in extragalactic turbulent magnetic fields: resulting energy spectrum and composition”. In: *A & A* 479, pp. 97–110. DOI: 10.1051/0004-6361:20078653. arXiv: 0709.1541.
- Gnedin, Nickolay Y., Andrea Ferrara, and Ellen G. Zweibel (2000). “Generation of the Primordial Magnetic Fields during Cosmological Reionization”. In: *The Astrophysical Journal* 539.2, p. 505. URL: <http://stacks.iop.org/0004-637X/539/i=2/a=505>.
- Greisen, Kenneth (1966). “End to the Cosmic-Ray Spectrum?” In: *Phys. Rev. Lett.* 16 (17), pp. 748–750. DOI: 10.1103/PhysRevLett.16.748. URL: <http://link.aps.org/doi/10.1103/PhysRevLett.16.748>.
- Hackstein, S. et al. (2016). “Propagation of ultrahigh energy cosmic rays in extragalactic magnetic fields: a view from cosmological simulations”. In: *MNRAS* 462, pp. 3660–3671. DOI: 10.1093/mnras/stw1903. arXiv: 1607.08872.
- Harari, D., S. Mollerach, and E. Roulet (2014). “Anisotropies of ultrahigh energy cosmic rays diffusing from extragalactic sources”. In: *Physical Review Letters* 89.12, 123001, p. 123001. DOI: 10.1103/PhysRevD.89.123001. arXiv: 1312.1366 [astro-ph.HE].
- Haverkorn, M. (2015). “Magnetic Fields in the Milky Way”. In: *Magnetic Fields in Diffuse Media*. Ed. by A. Lazarian, E. M. de Gouveia Dal Pino, and C. Melioli. Vol. 407. Astrophysics and Space Science Library, p. 483. DOI: 10.1007/978-3-662-44625-6_17. arXiv: 1406.0283.
- Hillas, A. M. (1984). “The Origin of Ultra-High-Energy Cosmic Rays”. In: *Annual Review of Astronomy and Astrophysics* 22.1, pp. 425–444. DOI: 10.1146/annurev.aa.22.090184.002233. eprint: <http://dx.doi.org/10.1146/annurev.aa.22.090184.002233>. URL: <http://dx.doi.org/10.1146/annurev.aa.22.090184.002233>.

References

- Hörandel, J. R. (2013). “Early cosmic-ray work published in German”. In: *American Institute of Physics Conference Series*. Ed. by J. F. Ormes. Vol. 1516. American Institute of Physics Conference Series, pp. 52–60. DOI: 10.1063/1.4792540. arXiv: 1212.0706.
- Kampert, K.-H. et al. (2013). “CRPropa 2.0 - A public framework for propagating high energy nuclei, secondary gamma rays and neutrinos”. In: *Astroparticle Physics* 42, pp. 41–51. DOI: 10.1016/j.astropartphys.2012.12.001. arXiv: 1206.3132 [astro-ph.IM].
- Khan, E. et al. (2005). “Photodisintegration of ultra-high-energy cosmic rays revisited”. In: *Astroparticle Physics* 23, pp. 191–201. DOI: 10.1016/j.astropartphys.2004.12.007. eprint: astro-ph/0412109.
- Kotera, K. and M. Lemoine (2008). “Optical depth of the Universe to ultrahigh energy cosmic ray scattering in the magnetized large scale structure”. In: *Physical Review Letters* 77.12, 123003, p. 123003. DOI: 10.1103/PhysRevD.77.123003. arXiv: 0801.1450.
- Kotera, K. and A. V. Olinto (2011). “The Astrophysics of Ultrahigh-Energy Cosmic Rays”. In: *ARA* 49, pp. 119–153. DOI: 10.1146/annurev-astro-081710-102620. arXiv: 1101.4256 [astro-ph.HE].
- Kotera, Kumiko and Martin Lemoine (2008). “Inhomogeneous extragalactic magnetic fields and the second knee in the cosmic ray spectrum”. In: *Phys. Rev. D* 77, p. 023005. DOI: 10.1103/PhysRevD.77.023005. arXiv: 0706.1891 [astro-ph].
- Kronberg, P P (1994). “Extragalactic magnetic fields”. In: *Reports on Progress in Physics* 57.4, p. 325. URL: <http://stacks.iop.org/0034-4885/57/i=4/a=001>.
- Kuempel, D. (2014). “Extragalactic Propagation of Ultra-High Energy Cosmic Rays”. In: *ArXiv e-prints*. arXiv: 1409.3129 [astro-ph.HE].
- Kurganov, A. and E. Tadmor (2000). “New High-Resolution Central Schemes for Nonlinear Conservation Laws and Convection-Diffusion Equations”. In: *Journal of Computational Physics* 160, pp. 241–282. DOI: 10.1006/jcph.2000.6459.
- Letessier-Selvon, A. and T. Stanev (2011). “Ultrahigh energy cosmic rays”. In: *Reviews of Modern Physics* 83, pp. 907–942. DOI: 10.1103/RevModPhys.83.907. arXiv: 1103.0031 [astro-ph.HE].
- Li, Zhi-Yun et al. (2010). “Lowering the Characteristic Mass of Cluster Stars by Magnetic Fields and Outflow Feedback”. In: *The Astrophysical Journal Letters* 720.1, p. L26. URL: <http://stacks.iop.org/2041-8205/720/i=1/a=L26>.
- Mucke, A. et al. (2000). “SOPHIA: Monte Carlo simulations of photohadronic processes in astrophysics”. In: *Comput. Phys. Commun.* 124, pp. 290–314. DOI: 10.1016/S0010-4655(99)00446-4. arXiv: astro-ph/9903478 [astro-ph].
- Nagano, M. and A. A. Watson (2000). “Observations and implications of the ultrahigh-energy cosmic rays”. In: *Reviews of Modern Physics* 72, pp. 689–732. DOI: 10.1103/RevModPhys.72.689.
- Neronov, A. and I. Vovk (2010). “Evidence for Strong Extragalactic Magnetic Fields from Fermi Observations of TeV Blazars”. In: *Science* 328, p. 73. DOI: 10.1126/science.1184192. arXiv: 1006.3504 [astro-ph.HE].

References

- Nitz, D. (2008). “The Northern Site of The Pierre Auger Observatory”. In: *International Cosmic Ray Conference* 5, pp. 889–892. arXiv: 0706.3940.
- Pierre Auger Collaboration (2012). “Large-scale Distribution of Arrival Directions of Cosmic Rays Detected Above 10^{18} eV at the Pierre Auger Observatory”. In: *ApJS* 203, 34, p. 34. DOI: 10.1088/0067-0049/203/2/34. arXiv: 1210.3736 [astro-ph.HE].
- Ptitsyna, K. V. and S. V. Troitsky (2010). “PHYSICS OF OUR DAYS Physical conditions in potential accelerators of ultra-high-energy cosmic rays: updated Hillas plot and radiation-loss constraints”. In: *Physics Uspekhi* 53, pp. 691–701. DOI: 10.3367/UFNe.0180.201007c.0723. arXiv: 0808.0367.
- Puget, J. L., F. W. Stecker, and J. H. Bredekamp (1976). “Photonuclear interactions of ultrahigh energy cosmic rays and their astrophysical consequences”. In: *ApJ* 205, pp. 638–654. DOI: 10.1086/154321.
- Shu, Chi-Wang and Stanley Osher (1988). “Efficient implementation of essentially non-oscillatory shock-capturing schemes”. In: *Journal of Computational Physics* 77.2, pp. 439–471. ISSN: 0021-9991. DOI: [http://dx.doi.org/10.1016/0021-9991\(88\)90177-5](http://dx.doi.org/10.1016/0021-9991(88)90177-5). URL: <http://www.sciencedirect.com/science/article/pii/0021999188901775>.
- Sigl, G., F. Miniati, and T. A. Enßlin (2004). “Ultrahigh energy cosmic ray probes of large scale structure and magnetic fields”. In: *Physical Review Letters* 70.4, 043007, p. 043007. DOI: 10.1103/PhysRevD.70.043007. eprint: astro-ph/0401084.
- Sorce, J. G. et al. (2016). “Cosmicflows Constrained Local UniversE Simulations”. In: *MNRAS* 455, pp. 2078–2090. DOI: 10.1093/mnras/stv2407. arXiv: 1510.04900.
- Subramanian, K. (2015). “The origin, evolution and signatures of primordial magnetic fields”. In: *ArXiv e-prints*. arXiv: 1504.02311.
- Takami, Hajime, Susumu Inoue, and Tokonatsu Yamamoto (2012). “Propagation of ultra-high-energy cosmic ray nuclei in cosmic magnetic fields and implications for anisotropy measurements”. In: *Astroparticle Physics* 35.12, pp. 767–780. ISSN: 0927-6505. DOI: <http://dx.doi.org/10.1016/j.astropartphys.2012.03.008>. URL: <http://www.sciencedirect.com/science/article/pii/S0927650512000618>.
- Taylor, A. M. (2014). “UHECR composition models”. In: *Astroparticle Physics* 54, pp. 48–53. DOI: 10.1016/j.astropartphys.2013.11.006. arXiv: 1401.0199 [astro-ph.HE].
- Tinyakov, P. G. and F. R. Urban (2015). “Full sky harmonic analysis hints at large ultra-high energy cosmic ray deflections”. In: *Soviet Journal of Experimental and Theoretical Physics* 120, pp. 533–540. DOI: 10.1134/S1063776115030231. arXiv: 1411.2486 [astro-ph.HE].
- Trivedi, P., K. Subramanian, and T. R. Seshadri (2014). “Primordial magnetic field limits from the CMB trispectrum: Scalar modes and Planck constraints”. In: *Physical Review Letters* 89.4, 043523, p. 043523. DOI: 10.1103/PhysRevD.89.043523. arXiv: 1312.5308 [astro-ph.CO].
- Vallée, Jacques P. (2004). “Cosmic magnetic fields - as observed in the Universe, in galactic dynamos, and in the Milky Way”. In: *New Astronomy Reviews* 48.10, pp. 763–841. ISSN:

References

- 1387-6473. DOI: <http://dx.doi.org/10.1016/j.newar.2004.03.017>. URL: <http://www.sciencedirect.com/science/article/pii/S138764730400065X>.
- Vazza, F. et al. (2014). “On the amplification of magnetic fields in cosmic filaments and galaxy clusters”. In: *Mon. Not. Roy. Astron. Soc.* 445.4, pp. 3706–3722. DOI: 10.1093/mnras/stu1896. arXiv: 1409.2640 [astro-ph.CO].
- Vazza, F. et al. (2015). “Forecasts for the detection of the magnetised cosmic web from cosmological simulations”. In: *Astron. Astrophys.* 580, A119. DOI: 10.1051/0004-6361/201526228. arXiv: 1503.08983 [astro-ph.CO].
- Véron-Cetty, M.-P. and P. Véron (2010). “A catalogue of quasars and active nuclei: 13th edition”. In: *A & A* 518, A10, A10. DOI: 10.1051/0004-6361/201014188.
- Widrow, L. M. et al. (2012). “The First Magnetic Fields”. In: *Science & Space Review* 166, pp. 37–70. DOI: 10.1007/s11214-011-9833-5. arXiv: 1109.4052.
- Xu, H. et al. (2009). “Turbulence and Dynamo in Galaxy Cluster Medium: Implications on the Origin of Cluster Magnetic Fields”. In: *ApJL* 698, pp. L14–L17. DOI: 10.1088/0004-637X/698/1/L14. arXiv: 0905.2196 [astro-ph.CO].
- Zatsepin, G.T. and V.A. Kuz'min (1966). “UPPER LIMIT OF THE SPECTRUM OF COSMIC RAYS”. In: *JETP Lett. (USSR) (Engl. Transl.)* Vol: 4.
- van Velzen, S. et al. (2012). “Radio galaxies of the local universe. All-sky catalog, luminosity functions, and clustering”. In: *A & A* 544, A18, A18. DOI: 10.1051/0004-6361/201219389. arXiv: 1206.0031 [astro-ph.CO].

List of Figures

4.1.	Schematic view on the observation of remnant showers of heavy UHECR nuclei in case of the ideal observer (top), a finite observer (center) and a magnetized observer (bottom).	15
4.2.	Volume filling factor of CMFs in the UCS (left) and CS (right). Shown are the differential (solid) and the cumulative filling factor (dash-dotted). The solid line is multiplied with $\times 0.1$ for more clarity. We also show the constraints given from observations, see Sec. 2.2. The left plot is taken from Hackstein et al. (2016).	17
4.3.	Slice of the simulated volume in the CS for the <i>primordial</i> (left) and the <i>astrophysical</i> model (right). Shown is an overlay of the gas density (red), the temperature (blue) and magnetic fields (green).	18
4.4.	Simulated path of propagation of five UHECR protons with final energy of 1 , 10 and 100 EeV (left to right) in the <i>primordial</i> model. Every color refers to a different particle.	18
5.1.	Normalized energy spectrum of UHECRs as injected at all sources (dashed) and recieved by the observer (solid) in the UCS in a pure iron injection scenario.	19
5.2.	Same as Fig. 5.1 in the CS in pure proton (left) and pure iron (right) injection scenarios.	20
5.3.	Same as Fig. 5.1 for particles above 10 EeV in the $B=0$ model and several injection scenarios of the CS. The error bars show the Poissonian noise for the single observer	21
5.4.	Average number of nucleons A of UHECRs as a function of energy as received by the observers in the UCS in scenarios with pure iron <i>mass halo</i> (left and right, blue) and <i>homogeneous</i> injection (right, green). The error bars show the 1σ standard deviation for the 18 observers.	22
5.5.	Same as Fig. 5.4 in the several injection scenarios of the CS. Left: comparison of the several magnetic field models. Right: particles above 10 EeV in the $B=0$ model. The error bars show the standard error for the single observer.	22
5.6.	Ratio of observed to injected number of particles per source as function of distance to the observer in the UCS in a pure iron injection scenario. We consider all particles above the displayed limit. We take the average over all 18 observers, the error bars show the 1σ standard deviation.	23
5.7.	Longest possible travelled distance of a charged particle in the lifetime of the universe in absence of magnetic fields (top) and under constant deflection (bottom).	24
5.8.	full-sky maps of arrival directions in the $B=0$ model for injection from <i>homogeneous</i> (left), <i>density</i> (center) and <i>mass halo</i> sources (right). All maps are shown for a minimum energy of 10 EeV of events.	25

List of Figures

5.9. Average angular power C_l as a function of minimum energy of observed UHE-CRs in the UCS in a pure iron injection scenario. The left plot compares different strength of EGMFs in a mass halo injection scenario, while the right plot compares mass halo to homogeneous injection in the strongest EGMF models. The shaded regions show the $1 - 3\sigma$ isotropic prediction.	26
5.10. Same as Fig. 5.9 in the CS in pure proton (left) and pure iron (right) injection scenarios.	27
5.11. Same as Fig. 5.10 in the $B=0$ model (more are on the way) and several injection scenarios of the CS.	28

A. Appendix

A.1. Energy Spectrum

```

; returns normalized spectrum of 'particle_energy'
; from 'min_energy' to 'max_energy'
FUNCTION CREATE_ENERGY_SPECTRUM, $
    particle_energy, min_energy, max_energy, bin_size
    spectrum = HISTOGRAM( ALOG10(particle_energy), $
        MIN=min_energy, MAX=max_energy, BINSIZE=bin_size)
; normalize spectrum by total number
    spectrum /= TOTAL(spectrum)
    RETURN, spectrum
END
; this function is called for the injected and the received energies

```

A.2. Composition

```

; creates the average composition and standard-deviation
PRO CREATE_COMPOSITION, $
    nuclear_masses, maximum_mass, $           ; input
    composition_average, composition_error     ; output
    composition = HISTOGRAM(nuclear_masses, $
        MIN=1, MAX=maximum_mass, BINSIZE=1)
; mass numbers of the corresponding bins
    mass = INDGEN(maximum_mass) + 1
    number = N_ELEMENTS(nuclear_masses)
; to calculate logarithmic mean and error
    composition = ALOG10(composition)
    composition_average = TOTAL(composition * mass) / number
    average = REBIN(composition_average, maximum_mass)
; standard error:  $\sqrt{TOTAL(x - \langle x \rangle)^2} / N$ 
    composition_error = $
        SQRT(TOTAL(composition * (mass - average)^2)) / number
END
; this procedure is repeated for masses in every energy bin

```


A.3. Source Contribution

```

; returns the average ratio of observed to injected particles
; from a single source as function of distance to source
; up to 'max_distance'
FUNCTION GET_SOURCE_CONTRIBUTION, $
    distance_injections, distance_sources, $
    injections_per_source, max_distance
    histogram_injections = HISTOGRAM(ALOG10([distance_injections]), $
        MIN=min_distance, MAX=max_distance, NBIN=nbin)
    histogram_sources = HISTOGRAM(ALOG10([distance_sources]), $
        MIN=min_distance, MAX=max_distance, NBIN=nbin)
; average contribution of sources at all distances
    contribution = histogram_injections $
        / (histogram_sources * injections_per_source)
    RETURN, contribution
END
; procedure repeated for all observers,
; average is calculated with MEAN(), standard deviation with STDDEV()

```

A.4. Angular Power

```

; to create the angular power, the following procedures are used
; - first the full sky map of arrival directions is produced
;   for all energy limits with use of CREATE_FULLSKY
; - from these we get the angular power spectrum C_l
;   with IANAFast of the healpix package:
;   IANAFast,healpix_fullsky,power_spectrum, /RING, /DOUBLE

; returns fullsky healpix map of arrival directions
FUNCTION CREATE_FULLSKY, $
    px,py,pz
    nside = 32 ; parameters for healpix map
    npix = 12*nside^2
; transform the invert momentum: cartesian -> spherical
    XYZ_TO_ANGLES,-px,-py,-pz,r,phi,theta, /RAD
; position of angle pairs in ring map
    ANG2PIX_RING, nside, theta, phi, ipring
; count events in same pixel
    ADDUP_ARRAY_TO_INDEX, ipring, ipring, npix, $
        sum, NUM=healpix_fullsky
    RETURN, healpix_fullsky
END

```

A. Appendix

```

; adds up entries in 'value' into 'sum' at the corresponding 'index'
; 'num' counts adds to 'sum' at 'index'
PRO ADDUP_ARRAY_TO_INDEX, $
    value, index, nsum, $ ; input
    sum, NUM=num          ; output
; prepare output arrays
    sum = DBLARR(nsum)
    num = sum
; sort 'index' and 'value' in temporary arrays
    sort = SORT(index)
    ix = index[sort]
    val = value[sort]
    REPEAT BEGIN
; find first entry for every pixel
        ixuniq = UNIQ(ix)
; add all these values at their pixel
        sum[ix[ixuniq]] += val[ixuniq]
; increase counter at those pixels
        num[ix[ixuniq]]++
; remove used indices and values from the temporary arrays
        val = REMOVE_ARRAY_ENTRY(val, ixuniq)
        ix = REMOVE_ARRAY_ENTRY(ix, ixuniq)
; until all entries are used
    ENDREP UNTIL N_ELEMENTS(ix) EQ 0
END

; returns smaller version of 'array',
; removes entries at indices in 'entry'
FUNCTION REMOVE_ARRAY_ENTRY, $
    array, entry
    RETURN, array[INDEX_COMPLEMENT(entry, N_ELEMENTS(array)-1)]
END

; returns all indices =< 'max' that are not found in 'index'
FUNCTION INDEX_COMPLEMENT, $
    index, max
    RETURN, WHERE(~HISTOGRAM([index], MIN=0, MAX=max, /NAN), /NULL)
END

```

Hiermit bestätige ich, dass die vorliegende Arbeit von mir selbständig verfasst wurde und ich keine anderen als die angegebenen Hilfsmittel - insbesondere keine im Quellenverzeichnis nicht benannten Internet-Quellen - benutzt habe und die Arbeit von mir vorher nicht einem anderen Prüfungsverfahren eingereicht wurde. Die eingereichte schriftliche Fassung entspricht der auf dem elektronischen Speichermedium. Ich bin damit einverstanden, dass die Masterarbeit veröffentlicht wird.

Hamburg, den 28. März 2017,